ORIGINAL RESEARCH

An Eco-Friendly Synthesis Approach for Enhanced Photocatalytic and Antibacterial Properties of Copper Oxide Nanoparticles Using *Coelastrella terrestris* Algal Extract

Manisha Khandelwal[1], Sunita Choudhary[2], Harish[2], Ashok Kumawat[3], Kamakhya Prakash Misra [ID][3], Yogeshwari Vyas[1], Bhavya Singh[4], Devendra Singh Rathore [ID][4], Kanchan Soni[3], Ashima Bagaria[3], Rama Kanwar Khangarot [ID][1]

[1]Department of Chemistry, University College of Science, Mohanlal Sukhadia University, Udaipur, Rajasthan, 313001, India; [2]Department of Botany, University College of Science, Mohanlal Sukhadia University, Udaipur, Rajasthan, 313001, India; [3]Department of Physics, School of Basic Sciences, Manipal University Jaipur, Jaipur, Rajasthan, 303007, India; [4]Department of Environmental Sciences, Mohanlal Sukhadia University, Udaipur, Rajasthan, 313001, India

Correspondence: Rama Kanwar Khangarot, Department of Chemistry, University College of Science, Mohanlal Sukhadia University, Udaipur, Rajasthan, 313001, India, Email ramakanwar@mlsu.ac.in

Background: In the current scenario, the synthesis of nanoparticles (NPs) using environmentally benign methods has gained significant attention due to their facile processes, cost-effectiveness, and eco-friendly nature.

Methods: In the present study, copper oxide nanoparticles (CuO NPs) were synthesized using aqueous extract of *Coelastrella terrestris* algae as a reducing, stabilizing, and capping agent. The synthesized CuO NPs were characterized by X-ray diffraction (XRD), UV-visible spectroscopy (UV-Vis), Fourier transform infrared spectroscopy (FTIR), dynamic light scattering (DLS), and field emission scanning electron microscopy (FE-SEM) coupled with energy-dispersive X-ray spectroscopy (EDS).

Results: XRD investigation revealed that the biosynthesized CuO NPs were nanocrystalline with high-phase purity and size in the range of 4.26 nm to 28.51 nm. FTIR spectra confirmed the existence of secondary metabolites on the surface of the synthesized CuO NPs, with characteristic Cu–O vibrations being identified around 600 cm^{-1}, 496 cm^{-1}, and 440 cm^{-1}. The FE-SEM images predicted that the enhancement of the algal extract amount converted the flattened rice-like structures of CuO NPs into flower petal-like structures. Furthermore, the degradation ability of biosynthesized CuO NPs was investigated against Amido black 10B (AB10B) dye. The results displayed that the optimal degradation efficacy of AB10B dye was 94.19%, obtained at 6 pH, 50 ppm concentration of dye, and 0.05 g dosage of CuO NPs in 90 min with a pseudo-first-order rate constant of 0.0296 min^{-1}. The CuO-1 NPs synthesized through algae exhibited notable antibacterial efficacy against *S. aureus* with a zone of inhibition (ZOI) of 22 mm and against *P. aeruginosa* with a ZOI of 17 mm.

Conclusion: Based on the findings of this study, it can be concluded that utilizing *Coelastrella terrestris* algae for the synthesis of CuO NPs presents a promising solution for addressing environmental contamination.

Keywords: green synthesis, CuO NPs, photocatalysis, antibacterial activity, wastewater treatment

Introduction

In recent years, inorganic nanoparticles (NPs) which include metal and metal oxide NPs have gained significant attention owing to their appealing chemical, physical, and biological properties.[1–7] These distinctive properties are shown by NPs due to their size, shape, stability, and large surface-to-volume ratio.[8–11] Among these NPs, copper oxide nanoparticles (CuO NPs) are currently one of the most competitive materials due to their characteristic properties, such as abundance, inexpensiveness, biocompatibility, and remarkable photonic efficiency.[12–14] These CuO NPs have found extensive

Graphical Abstract
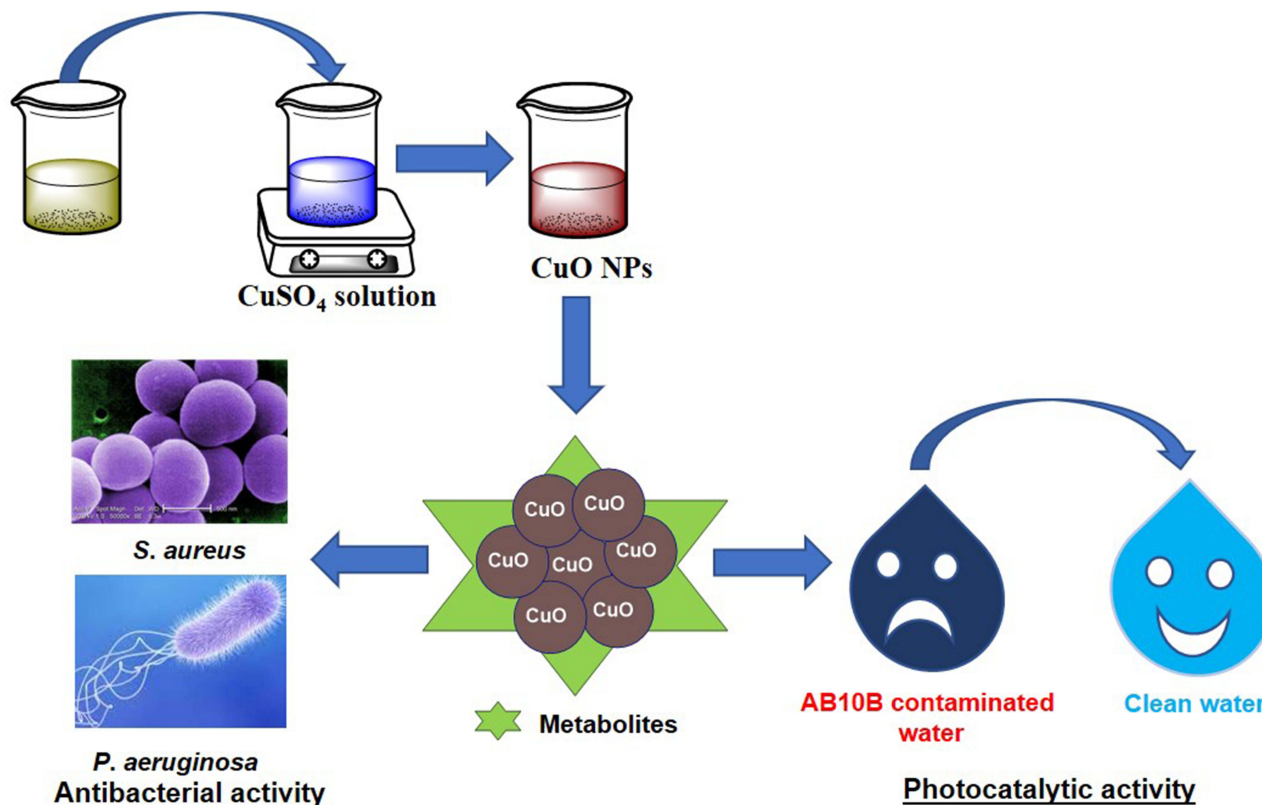
application across diverse fields, including catalysis, photocatalysis, wastewater treatment, sensors, environmental remediations, and biomedical.[15–17]

Traditionally, CuO NPs are synthesized via chemical and physical methods.[18,19] Chemical methods encompass techniques such as chemical vapour deposition,[18] laser pyrolysis,[20] and sol-gel method,[21] etc. and physical methods include ball milling,[22] physical vapour deposition,[23] pulse laser ablation,[24] and lithography.[25] However, these conventional synthesis methods consume high energy and use toxic chemicals, raising environmental concerns.[26] To address these challenges, more environmentally sustainable methods are required that utilize natural resources such as plants,[27] algae,[28] bacteria,[29] and fungi,[30] for the synthesis of CuO NPs. These methods offer distinct advantages in terms of stability, compatibility, safety, and cost-effectiveness. Plants and micro-organisms (for example, algae, bacteria, fungi) contain phytochemicals, i.e., polyphenols, tannins, alkaloids, terpenoids, saponins, carotenoids, flavonoids, etc., that could function as reducing, stabilizing, and capping agents for the synthesis of CuO NPs with varied compositions, shapes, and sizes.[31–34] Notably, algae have garnered attention as a viable source for the synthesis of CuO NPs due to their facile cultivation in laboratory settings and the presence of phytochemicals.[35] The phytochemicals contained by algae are carbohydrates, terpenoids, ketones, steroids, fatty acids, flavonoids, alkaloids, phenolics, etc.[36–38] These phytochemicals are responsible for the reduction, capping, and stabilization of CuO NPs.[39] The NPs synthesized from algae have long-time stability and broad applications in diverse fields.[40] The shape, size, and stability of CuO NPs depend on various parameters, such as pH, temperature, incubation time, concentration of algal extract, and concentration of copper salt precursor.[41] There are few reports present in the literature on the biosynthesis of CuO NPs through algae, as represented in Table 1.

Despite the progress in the biosynthesis methods, there remains a gap in the literature regarding the synthesis of CuO NPs utilizing *Coelastrella terrestris*, a species of green algae. This research aims to address this gap by investigating the

Table 1 List of Algal Strains Used in the Biosynthesis of CuO NPs

S. No.	Algal Species	Shape of CuO NPs	Size (nm)	Applications	References
1.	*Bifurcaria bifurcata*	Spherical and elongated	5–45	Antibacterial activity	[42]
2.	*Sargassum polycystum*	–	–	Antimicrobial and anticancer activity	[28]
3.	*Cystoseira trinodis*	Spherical	6–7.8	Antibacterial, antioxidant, and photocatalytic activity	[43]
4.	*Anabaena cylindrica*	Rod-like	3.6	Antimicrobial activity and toxicity evaluation	[44]
5.	*Macrocystis pyrifera*	Spherical	2–50	–	[45]
6.	*Sargassum longifolium*	Spherical	40–60	Antibacterial and antioxidant activity	[46]
7.	*Asterarcys quadricellulare*	Flower petals and flattened rice	4.76–13.70	Photocatalytic activity	[47]

biosynthesis of CuO NPs using *Coelastrella terrestris* and exploring the impact of various reaction parameters on nanoparticle synthesis. The objectives of this study are to optimize the biosynthesis parameters for CuO NPs, characterize the synthesized NPs using advanced techniques such as X-ray diffraction (XRD), Fourier-transform infrared spectroscopy (FTIR), UV-Vis spectroscopy (UV-Vis), and field emission scanning electron microscopy (FE-SEM) coupled with energy-dispersive X-ray spectroscopy (EDS), and evaluate the photocatalytic and antibacterial properties of the synthesized CuO NPs. The efficacy of the synthesized CuO NPs as photocatalysts will be assessed through the degradation of Amido black 10B (AB10B) dye, while their antibacterial activity will be evaluated against both Gram-positive and Gram-negative bacterial strains.

By addressing these objectives, this study aims to contribute to the development of sustainable and effective NPs for applications in environmental and biomedical domains. The findings of this research hold significant implications for advancing the field of NPs synthesis and its practical utilization in addressing environmental and health-related challenges.

Experimental Section

The materials and methods used for the biological and chemical synthesis of CuO NPs, photocatalytic experiments, and antibacterial analysis are discussed in detail in Supplementary Material 1. Algal-mediated CuO NPs were synthesized by varying a single parameter while keeping others constant. Throughout the manuscript, convenient notations are used for clarity. Specifically, CuO-1, CuO-2, and CuO-3 denote CuO NPs synthesized from 15 mL, 20 mL, and 25 mL volumes of algal extract, respectively. The notation CuO-4 refers to CuO NPs synthesized using the chemical synthesis method. Figure 1 provides a schematic representation of both the biological and chemical processes involved in the synthesis of CuO NPs.

Photocatalytic Degradation of AB10B Dye

The photocatalytic activity of CuO NPs was observed by studying the degradation of AB10B using visible light illumination with a commercial 60 W tungsten filament bulb (Philips). A cutoff water filter was applied to eliminate any other radiations except visible light. 0.05 g of CuO NPs photocatalyst powder was dispersed in 40 mL AB10B dye solution and placed in a dark condition and stirred slowly for 30 min to establish an adsorption/desorption equilibrium. The photocatalytic activity started when the solution was illuminated with a source, and the sample of the solution was taken out after 15 min using a dropper carefully so that the catalyst particles did not interfere. The photodegradation rate was evaluated by assessing the absorbance at 618 nm by a UV-Vis spectrophotometer. The parameters, such as the pH of the dye solution, the concentration of dye, and the amount of catalyst, were varied to achieve optimum conditions. The pH of the solution was altered by adding 0.1 N H_2SO_4 and 0.1 N NaOH solutions that had been previously standardized.
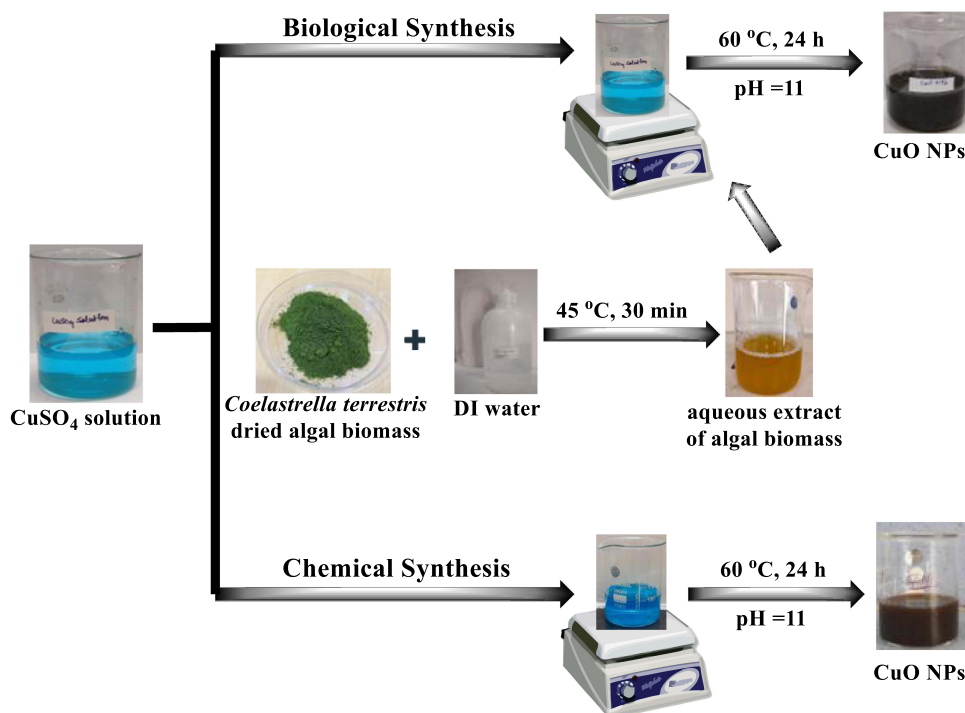
Figure 1 Schematic illustration of the biological and chemical synthesis of CuO NPs.

All photocatalytic experiments were performed twice for clarity and perfection. The percentage of dye degradation is calculated according to equation (1).

$$\% \text{ degradation} = \frac{(C_0 - C_t)}{C_0} \times 100 \qquad (1)$$

Where C_o = initial concentration of AB10B dye before exposure to visible light irradiation; C_t = concentration of AB10B dye at a specific time t.

Equation (2) of the first-order plot was used to calculate the photodegradation rate constant (k), assuming pseudo-first-order kinetics.

$$\ln(C_0/C_t) = kt \qquad (2)$$

Results and Discussion
Effect of pH
An investigation was carried out, in order to determine how the reaction pH influences the synthesis of CuO NPs from algal extract. The synthesis of CuO NPs was observed at an alkaline pH. While the synthesis of CuO NPs was not detected at acidic and neutral pH of the mixture of the algal extract and copper sulphate solution. Similar results were also observed by Banerjee and co-authors.[44] Hence, a pH of 11 was maintained throughout this experiment for the formation of CuO NPs. In the alkaline medium, the reducing and stabilizing capacity of *Coelastrella terrestris* algae was enhanced.[44]

Effect of Temperature
At room temperature (27°C), the synthesis of copper hydroxide nanoparticles (Cu(OH)$_2$ NPs) was observed. When the reaction temperature increased from 27°C to 60°C, the colour of the reaction mixture changed from blue to brown. This confirmed that CuO NPs were synthesized. This showed that the reaction temperature was a critical parameter for the synthesis of CuO NPs.

Effect of Algal Extract Volume

It was observed that algal extract concentration played an important role and was responsible for building the shape and size of CuO NPs. With increasing algal extract volume, the particle size of synthesized CuO NPs increased. The XRD analysis along the highest intensity plane (111) revealed that the CuO NPs formed at 15 mL of algal extract had a particle size of 7.62 nm, which increased to 8.49 nm and 8.61 nm at 20 mL and 25 mL of algal extract, respectively. This infers that the size of CuO NPs expands with an increase in the volume of algal extract (reducing, capping, and stabilizing agents).

Proposed Mechanism of CuO NPs Synthesized from *Coelastrella terrestris* Algae

The algal extract consists of biomolecules like proteins, enzymes, carbohydrates, lipids, polysaccharides, and secondary metabolites- terpenoids, alkaloids, and polyphenols which catalyze the synthesis of CuO NPs. Initially, the biocomponents existing in the aqueous algal extract acted as bioreductants and were responsible for reducing Cu(II) to Cu(0), which formed CuO NPs via a nucleation step.[48] After that, crystal growth continued till the CuO NPs achieved a stable shape and size.[49] A plausible mechanism of algal-mediated biosynthesis of CuO NPs illustrated in Figure 2.

XRD Analysis

Figure 3 depicts the XRD patterns of CuO NPs synthesized by biological and chemical methods. A comparison of the XRD patterns of CuO NPs with the standard JCPDS card no. 80–1916[50] and 48–1548[51] confirmed the crystalline monoclinic and end-centered nature, as evidenced by the peaks at 2θ values of 32.48°, 35.49°, 38.69°, 48.66°, 53.41°, 58.25°, 61.46°, 66.14°, and 68.01°, which indexed to (110), (−111), (111), (202), (020), (202), (113), (−311), and (220)
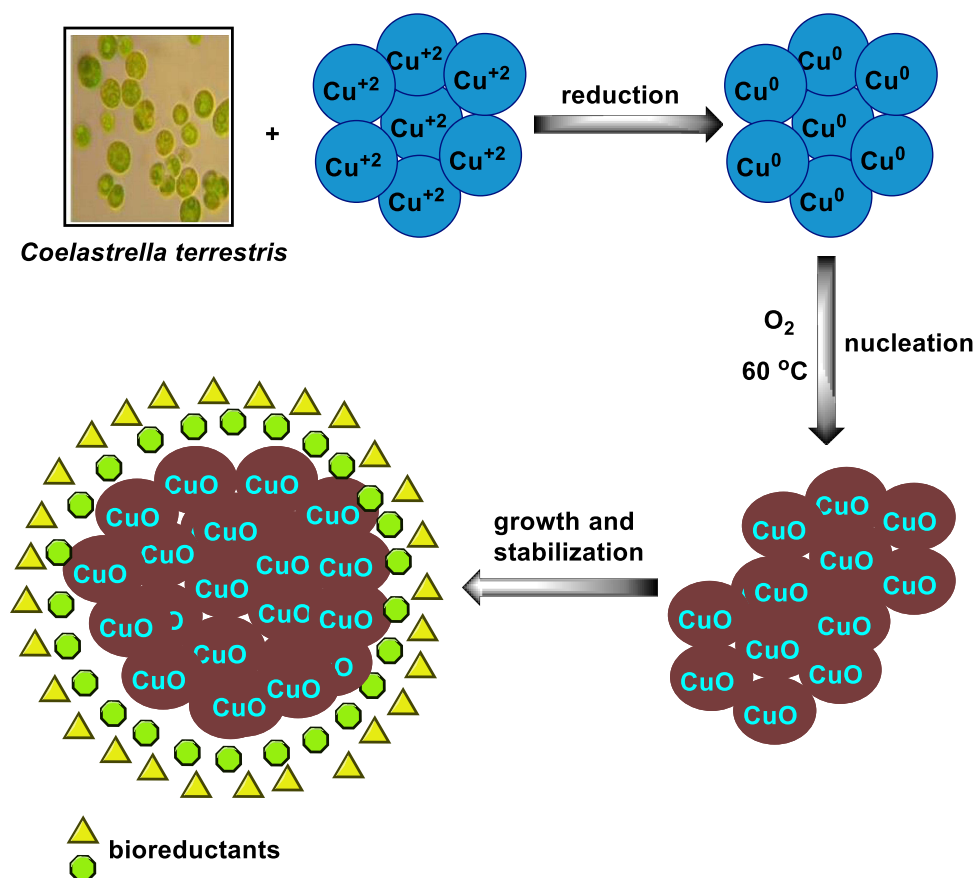

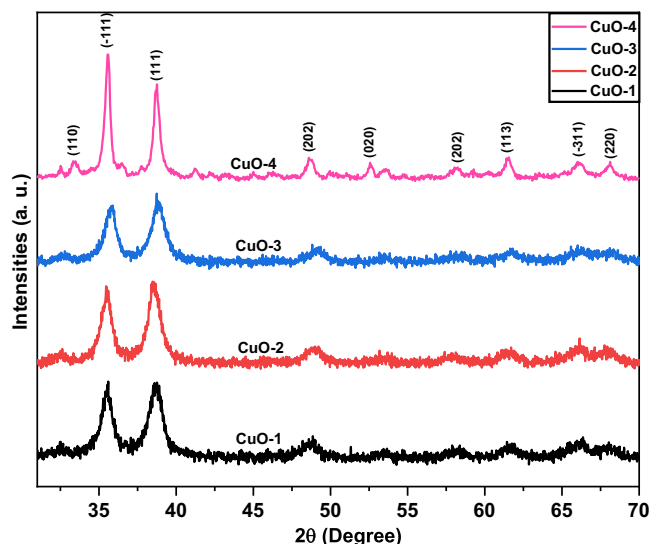**Figure 2** A plausible mechanism of algal-mediated biosynthesis of CuO NPs.

Figure 3 XRD patterns of the biosynthesized CuO NPs (CuO-1, CuO-2, and CuO-3) and chemically synthesized CuO NPs (CuO-4).

planes, respectively. No additional peak was observed in all four samples, which indicated that the synthesized CuO NPs were phased pure.

Orientation Parameter

The orientation parameter ($\gamma_{(hkl)}$) refers to the extent to which the crystallites align along a specific crystallographic plane. Equation (3) was used to evaluate the orientation parameter of the synthesized CuO NPs for a particular plane with Miller indices (hkl).[52]

$$\gamma_{hkl} = \frac{I_{hkl}}{I_{110} + I_{-111} + I_{111} + I_{202} + I_{020} + I_{202} + I_{113} + I_{-311} + I_{220}} \tag{3}$$

where $I_{(hkl)}$ indicates the intensity of associated planes with Miller indices (hkl). Calculated orientation parameter values are given in Table 2. It can be noticed that $\gamma_{(hkl)}$ valued decrease along (110) plane as we move from CuO-1 to CuO-4 and it increase along (111) plane with an exception of CuO-4. It means the enhancement in the amount of algal extract degrades the crystal growth of CuO NPs along the (110) plane and improves it along the (111) plane. Rest, along all other planes, the $\gamma_{(hkl)}$ values are random and irregular. Such variation of $\gamma_{(hkl)}$ along other crystallographic planes indicates the random growth and distribution of particles.

Crystallite Size and Strain

Using the Scherer equation (4), the crystallite size of the samples was calculated from the XRD peak.[53]

Table 2 Orientation Parameters Along Distinct Crystallographic Planes

S. No.	Orientation Parameters ($\gamma_{(hkl)}$)								
	Sample Name	(110)	(−111)	(111)	(202)	(020)	(202)	(113)	(−311)	(220)
1.	CuO-1	0.0857	0.2013	0.1994	0.0964	0.0727	0.0788	0.0860	0.0947	0.0848
2.	CuO-2	0.0806	0.2015	0.2107	0.0857	0.0775	0.0725	0.0837	0.1005	0.0872
3.	CuO-3	0.0799	0.1888	0.2166	0.0955	0.0751	0.0789	0.0853	0.0933	0.0864
4.	CuO-4	0.0746	0.2678	0.2132	0.0824	0.0722	0.0620	0.0824	0.0717	0.0735

Table 3 Strain and Crystallite Size of Synthesized CuO NPs, Calculated by the Scherrer Equation Along Different Planes and the W-H Plot

S. No.	Sample Name	Crystallite Size (t_S)									t_{WH}	Micro-Strain (ε)
		(110)	(−111)	(111)	(202)	(020)	(202)	(113)	(−311)	(220)		
1.	CuO-1	7.59	9.50	7.62	6.90	13.54	11.98	9.10	5.81	8.04	8.83	0.0010
2.	CuO-2	7.14	9.11	8.49	5.24	11.46	4.37	5.24	11.35	**4.26**	16.71	0.0151
3.	CuO-3	6.12	8.59	8.61	6.38	**28.51**	25.58	7.62	7.66	9.16	6.00	−0.0089
4.	CuO-4	17.17	20.38	17.62	14.46	19.07	11.03	13.63	9.67	12.43	86.68	0.0095

Notes: The bold value indicates the lowest and highest crystallite size calculated using the Scherrer equation.

$$t_S = \frac{k\lambda}{\beta \cos\theta} \tag{4}$$

Where t_S, k, λ, β, and θ denote the crystallite size of the NPs, Scherrer's constant (0.9), the wavelength of X-ray (0.1541 nm), full width at half maximum (FWHM) of diffraction peaks, and Bragg's angle of diffraction, respectively. The calculated crystallite size is displayed in Table 3. The crystallite size of the CuO NPs synthesized from algal extract lies in the range of 4.26 nm to 28.51 nm, as obtained by equation (4). The outcomes disclosed that CuO NPs synthesized from varied volumes of algal extract had a nanocrystalline nature and different particle sizes. Regular decrement along the (110) plane and increment along the (111) of the particle size could be noticed in Table 3. Hence, it is plausible to conclude that the synthesis route and enhancement of algal extract can affect the nucleation, and crystal growth, eventually governing the size of the biosynthesized CuO NPs. The chemically synthesized CuO NPs (CuO-4) disclosed a crystallite size of 20.38 nm along the highest intensity plane (−111).

Williamson-Hall analysis plays a vital role in the analysis of crystallite size and micro-strain. A linear fit to the curve $\beta\cos\theta$ versus $\sin\theta$ was compared with the equation (5) shown below.[54]

$$\beta\cos\theta = \frac{C\lambda}{t_{WH}} + 2\varepsilon\sin\theta \tag{5}$$

Where β is the FWHM corresponding to Bragg's peak, C is the correction factor (0.9), λ is the wavelength, t_{WH} is the crystallite size, and ε is the micro-strain. In the inset of the W-H plot (Figure 4), the equation of trend-line fit is represented along with the regression factor (R^2). Figure 4 demonstrated that the data points deviated significantly from the trend-line fit, showing uncertainties that are represented by the standard error bars. The calculated value of micro-strain (ε) and crystallite size (t_{WH}) were given in Table 3 to understand the quantitative view of the strain on crystallite size. The micro-strain increased in the CuO NPs with a higher volume of algal extract. The enhancement of the micro-strain might have implications for evolving certain structures, which will be discussed in a further section. Two types of micro-strains present here, compressive and tensile, were respectively denoted by negative and positive signs.

Dislocation Density

The dislocation density $\delta_{(hkl)}$ of all the samples along each plane was evaluated using equation (6) and tabulated in Table 4. The dislocation increased along the (110) plane while they decreased along (111) for algal-mediated CuO NPs. The random variation of $\delta_{(hkl)}$ was observed for all other crystallographic planes.

$$\delta_{(hkl)} = \frac{1}{(t_s)^2} \tag{6}$$

Size Estimation Using Dynamic Light Scattering (DLS)

DLS was performed to analyze the hydrodynamic size of CuO NPs. Figure 5 shows the distribution of the biosynthesized (*Coelastrella terrestris* algae) and chemically synthesized CuO NPs. The average particle sizes of CuO-1, CuO-2, CuO-3,
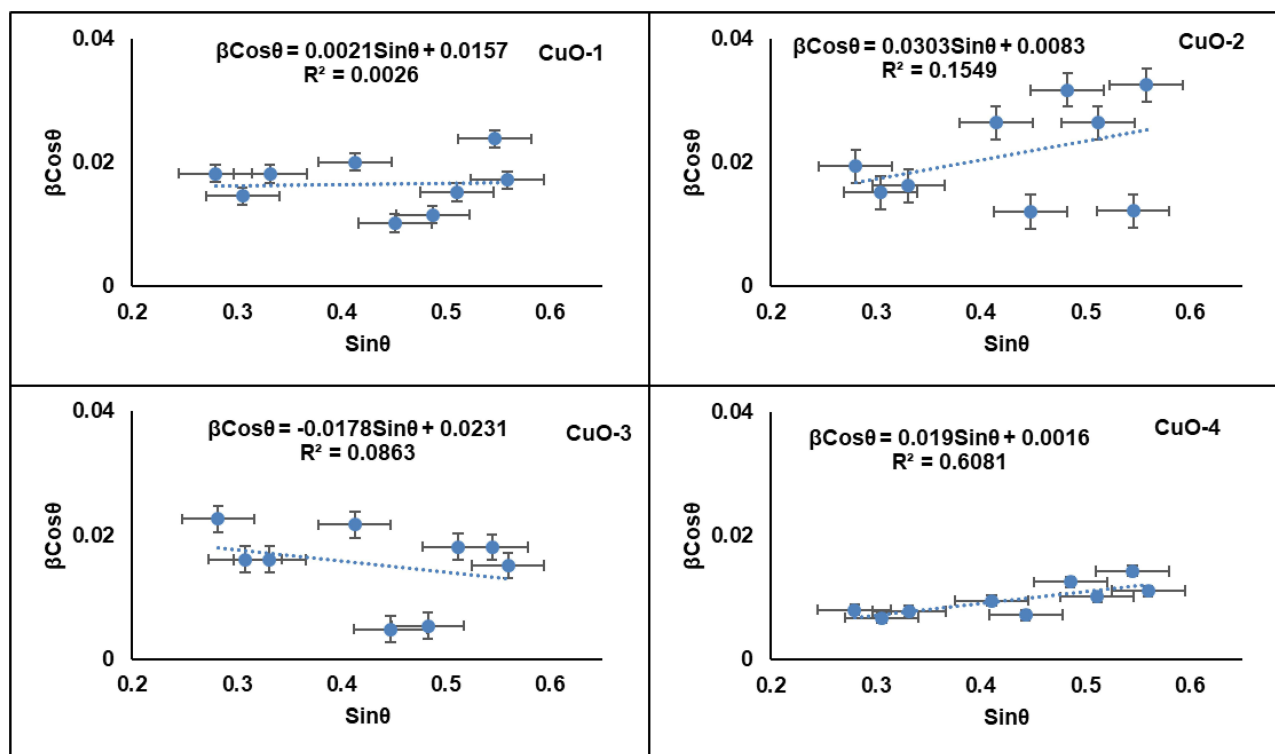
Figure 4 W-H plot of the biosynthesized CuO NPs (CuO-1, CuO-2, and CuO-3) and chemically synthesized (CuO-4). The standard error bars demonstrate the uncertainties.

and CuO-4 were 383.2, 457.9, 499.8, and 1092 nm, respectively. The observed particle size was higher than the sizes estimated by XRD because the attained size was not only associated with the core of the CuO NPs but also with the size of biomaterial adsorbed on the surface of the biosynthesized CuO NPs and the electrical double-layer (solvent wall) that flowed between the NPs. The hydrodynamic size of all the biosynthesized CuO NPs inferred the agglomeration of the particles. The particle agglomeration also influenced the photocatalytic activity of biosynthesized NPs. As the agglomeration in NPs was enhanced, their photocatalytic activity was reduced because of a decrease in penetration depth of the visible light radiations inside the agglomerates of NPs.[55,56]

FTIR Spectra

FTIR study was performed to recognize the biomolecules present in the *Coelastrella terrestris* algae and biosynthesize CuO NPs (CuO-1, CuO-2, and CuO-3). The FTIR spectra of *Coelastrella terrestris* algae, biosynthesized, and chemically synthesized CuO NPs are shown in Figure 6, and the wavenumber and associated functional groups are described in Table 5. The spectra of both samples exhibit prominent resemblance, with only minor shifts observed in the peak

Table 4 Dislocation Density ($\delta_{(Hkl)}$) Along Diverse Crystallographic Planes

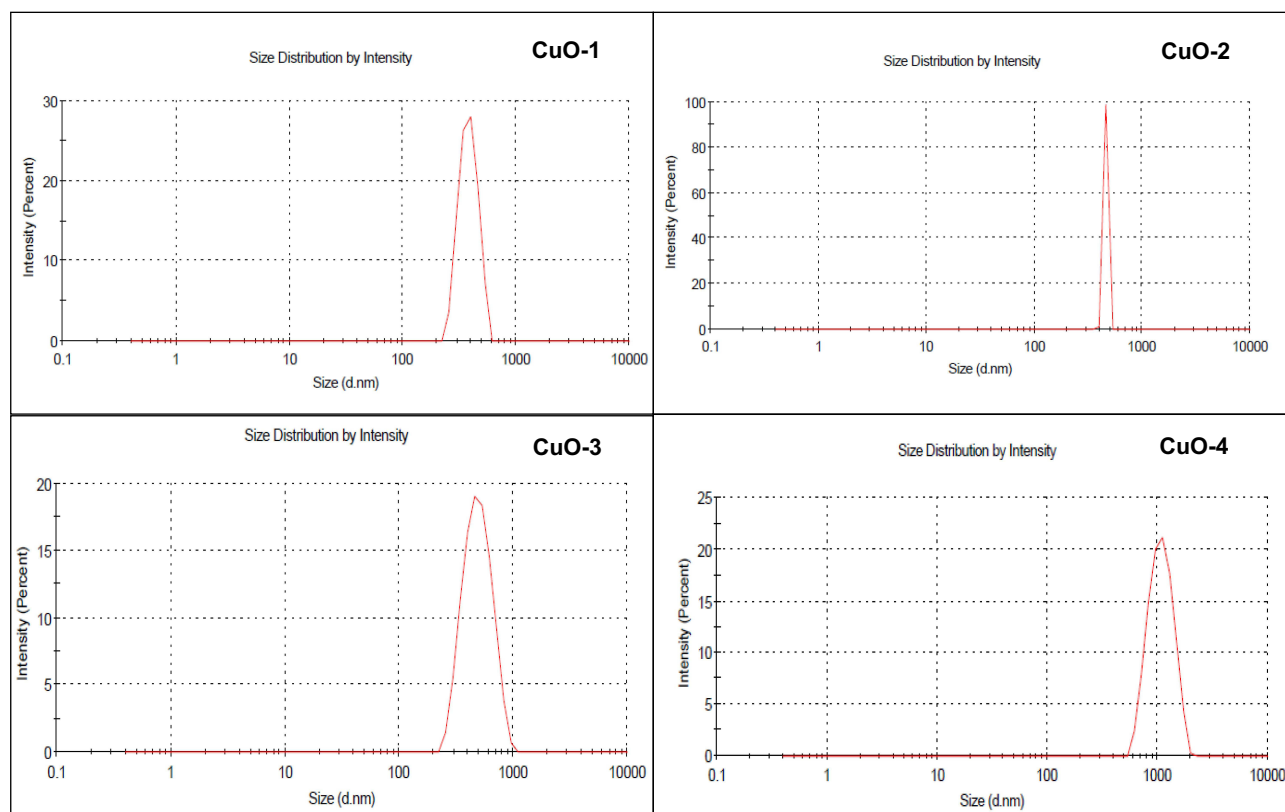| S. No. | | $\delta_{(hkl)}$ x 10^{15} m^{-2} | | | | | | | | |
|---|---|---|---|---|---|---|---|---|---|
| | Sample Name | (110) | (−111) | (111) | (202) | (020) | (202) | (113) | (−311) | (220) |
| 1. | CuO-1 | 0.0173 | 0.0111 | 0.0172 | 0.0210 | 0.0054 | 0.0070 | 0.0121 | 0.0296 | 0.0155 |
| 2. | CuO-2 | 0.0196 | 0.0120 | 0.0139 | 0.0364 | 0.0076 | 0.0524 | 0.0364 | 0.0077 | 0.0551 |
| 3. | CuO-3 | 0.0267 | 0.0135 | 0.0135 | 0.0246 | 0.0012 | 0.0015 | 0.0172 | 0.0170 | 0.0119 |
| 4. | CuO-4 | 0.0034 | 0.0024 | 0.0032 | 0.0048 | 0.0027 | 0.0082 | 0.0054 | 0.0107 | 0.0065 |

Figure 5 Particle size analysis using DLS of the biosynthesized CuO NPs (CuO-1, CuO-2, and CuO-3) and chemically synthesized CuO NPs (CuO-4).
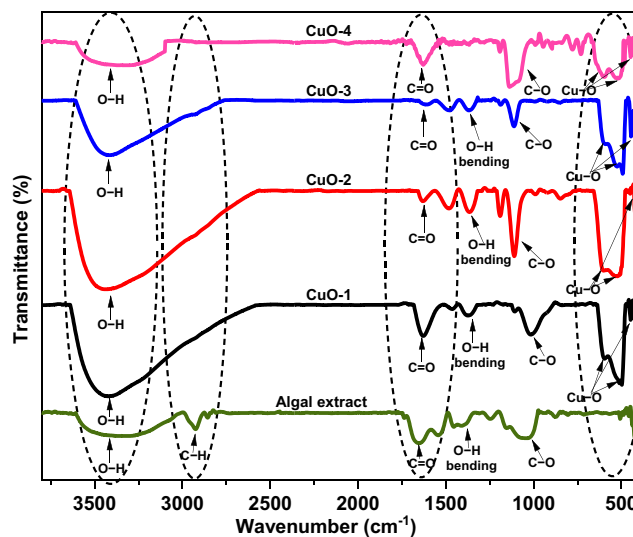

Figure 6 FTIR spectra of algal extract, biosynthesized CuO NPs (CuO-1, CuO-2, and CuO-3), and chemically synthesized CuO NPs (CuO-4).

positions, as indicated by the peak wavenumber. This similarity in bands with the marginal band shifts confirms the function of *Coelastrella terrestris* algal extract as a reducing, capping, and stabilizing agent in the biosynthesis of CuO NPs.[39] For example, the –N–H and –O–H stretching band of amines, alcohols, and phenols at 3430 cm^{-1} in the algal extract was shifted to 3439 cm^{-1}, 3451 cm^{-1}, and 3440 cm^{-1} for the CuO-1, CuO-2, and CuO-3, respectively.[57,58] The small peak at 2921 cm^{-1} in algal extract was associated with –C–H stretching of lipids and carbohydrates, while this peak was absent in all biosynthesized CuO NPs.[57] The –C=O stretching peak of amide at 1654 cm^{-1} in the algal extract was

Table 5 Functional Group Analysis of *Coelastrella terrestris* Algae, Biosynthesized CuO NPs (CuO-1, CuO-2, and CuO-3) and Chemically Synthesized CuO NPs (CuO-4) Through FTIR

Algae Wavenumber (cm^{-1})	CuO-1 Wavenumber (cm^{-1})	CuO-2 Wavenumber (cm^{-1})	CuO-3 Wavenumber (cm^{-1})	CuO-4 Wavenumber (cm^{-1})	Assigned Functional Groups
3430	3439	3451	3440	3359	v(O–H) stretching of moisture, alcohols, and phenols v(N–H) stretching of amines
2921	–	–	–	–	v(C–H) stretching of lipids and carbohydrates
1654	1627	1629	1611	1629	v(C=O) stretching of amides and absorbed CO_2
1537	1467	1494	1482	–	v(N–H) bending and v(C–N) stretching of amides
1395	1365	1365	1365	–	v(O–H) bending of carboxylic acids and alcohols
1048	1014	1113	1116	1119	v(C–O) of carbohydrates
–	608	608	605	600	v(Cu–O) of CuO NPs
–	500	528	494	515	v(Cu–O) of CuO NPs
–	448	423	445	430	v(Cu–O) of CuO NPs

shifted towards lower wavenumber 1627 cm^{-1}, 1629 cm^{-1}, 1611 cm^{-1} in CuO-1, CuO-2, and CuO-3, respectively.[31] The peak at 1629 cm^{-1} in CuO-4 was associated with atmospheric CO_2. The peak at 1537 cm^{-1} in the algal extract was shifted to 1467 cm^{-1}, 1494 cm^{-1}, 1482 cm^{-1} in CuO-1, CuO-2, and CuO-3, respectively. This peak was attributed to the v(N–H) bending and v(C–N) stretching of the amide group of protein.[57] The peaks at 1360–1450 cm^{-1} were attributed to the –OH bending of carboxylic acid and alcohol. The band at 1190 cm^{-1} was ascribed to C–H bending (aromatic in the plane).[59] Peak around 1024 cm^{-1} attributed to the –C–O bond of polyols and carbohydrates such as flavonoids, polysaccharides, terpenoids, etc. of algae.[60] These peaks demonstrated that metabolites present in algae, such as terpenoids, glycosides, polysaccharides, carbohydrates, lipids, proteins, flavonoids, phenols, and tannins, which include functional groups like ketones, aldehydes, carboxylic acids, and amide had covered the surfaces of the CuO NPs.[61,62] All synthesized CuO NPs showed the characteristic peak of the Cu–O bond, which was observed around 608 cm^{-1}, 500 cm^{-1}, and 440 cm^{-1}.[63,64]

Tauc's Plot

As illustrated in Figure 7, the band gap value of synthesized CuO NPs was analyzed by Tauc's plot. The Tauc's plot was drawn using the expression (7)[65,66] as follows:

$$(\alpha h\nu)^{1/n} = A(h\nu - E_g) \tag{7}$$

Where α represents the adsorption coefficient, A represents the proportionality constant, hν represents the incident light frequency, and E_g represents the band gap value. The type of transition is governed by the value of exponent "n"; n = ½ related to direct transition and n = 2 related to indirect transition. CuO NPs' direct transition was determined by extrapolating the linear section of the curve to the hν axis.[67] The estimated band gaps were 2.40 eV, 3.31 eV, 3.74 eV, and 3.90 eV for CuO-1, CuO-2, CuO-3, and CuO-4, respectively. The observed band gap values were higher than the bulk CuO powder (1.2 eV). Among all the synthesized CuO NPs, CuO-1 showed the lowest value of band gap, which demonstrated the superior photocatalytic activity of CuO-1 for the degradation of AB10B dye.
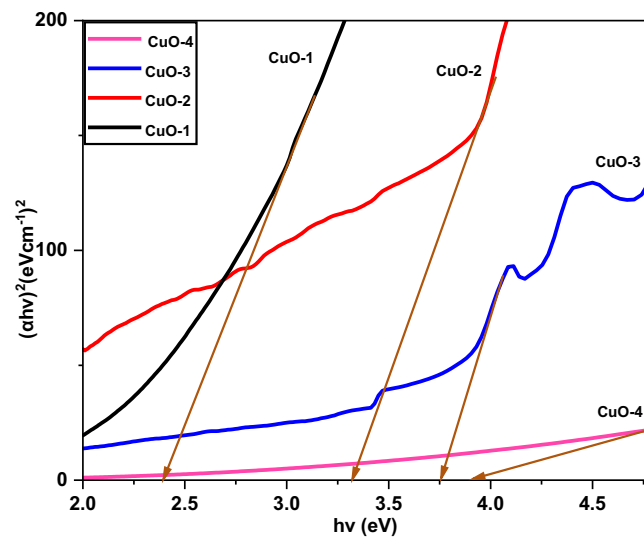
Figure 7 Tauc's plot of the biosynthesized CuO NPs (CuO-1, CuO-2, and CuO-3) and chemically synthesized CuO NPs (CuO-4).

FE-SEM and EDS Analysis

The FE-SEM image of the biosynthesized CuO NPs is depicted in Figure 8. Flattened rice-like structures were visible in CuO-1 where the least amount of algal extract was used. Enhancement of the algal extract during the nucleation process clubbed the flattened rice-like structures to flower petals. Flowers closely matching to the shape of the hibiscus were evolved. The flower structure can be considered as a kind of nanoassembly that has evolved probably because of the heterogeneous nucleation process. The heterogeneous nucleation process is promoted by the organic complexes formed during the biosynthesis of CuO NPs.[68] It can be concluded that the preferred orientation/shaping and assembly of nanostructures greatly depend on the composition of the algal extract. The evolution of nanoassembly (flower) is shown
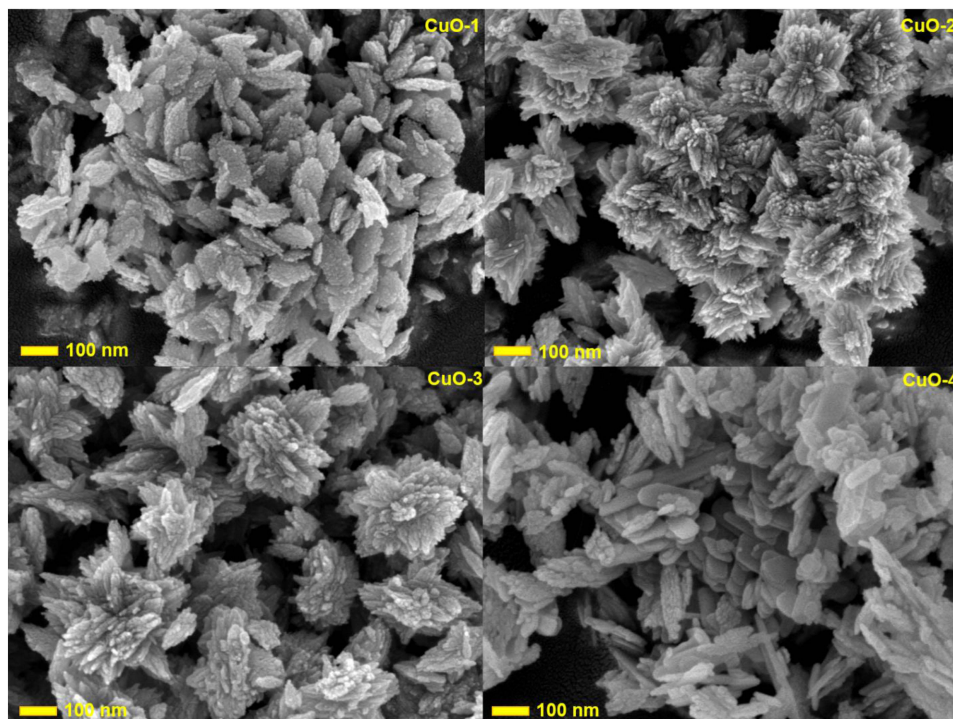

Figure 8 FE-SEM image of the biosynthesized CuO NPs (CuO-1, CuO-2, and CuO-3) and chemically synthesized CuO NPs (CuO-4).
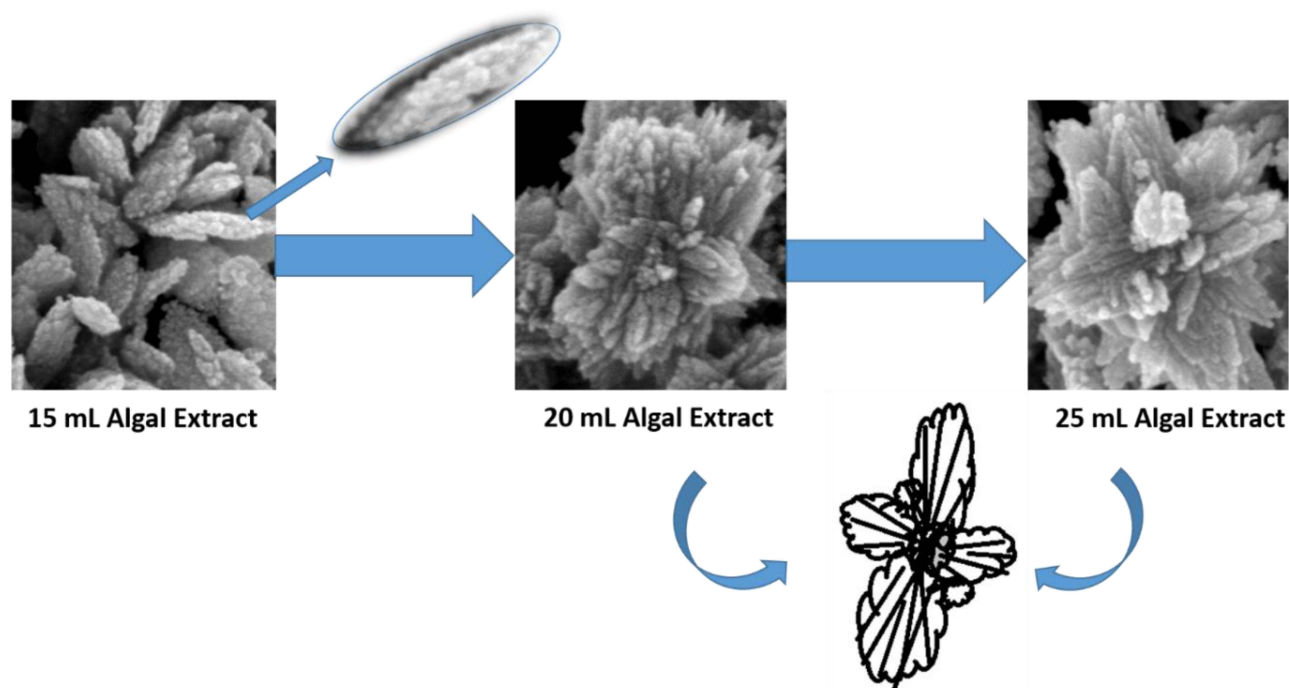
4147

Figure 9 Evolution of CuO nanostructure into the nanoassembly (flower).

in Figure 9. CuO-3 had a clear formation of the nanoassembly into the shape of a hibiscus flower. It might be because of the change in the nature of the micro-strain. As revealed by the W-H method, CuO-3 was under tensile strain. CuO-4, i.e., chemically synthesized NPs show the platelet structure which is broadly similar to those of CuO-1. There are the occasional formations of rod-like structures as well.

The chemical composition of biosynthesized CuO NPs studied by EDS analysis is shown in Figure 10. The EDS spectra of synthesized CuO NPs revealed strong peaks of copper (Cu) and oxygen (O). The presence of phytochemicals in the algal extract solution is responsible for the carbon (C) and sulphur (S) weak peaks.[44,69]

Photocatalytic Dye Degradation

Removal of dye using a photocatalyst is associated with adsorption and photocatalytic processes.[70] AB10B was selected due to its excessive use in biochemical research to stain for proteins and in criminal investigations to detect blood present with latent fingerprints.[71,72] It is reported that this dye is highly toxic to humans and damages the respiratory system, and also adversely affects the skin and eyes.[73,74] Therefore, it is important to develop a systematic process to eradicate AB10B dye from wastewater. The selected AB10B dye has colour index (C.I.) numbers 20470. The structure of AB10B dye is shown in Figure 11. A sequence of experiments was carried out to find the optimum condition for the degradation of AB10B dye using the CuO nanocatalyst under visible light.

Optimization of Reaction Parameters in the Degradation of AB10B Dye

The photodegradation of AB10B dye was measured from UV-visible spectra at the maximum absorbance wavelength (λ_{max}) peak at 618 nm. This peak was detected due to the presence of an azo chromophore (–N=N–). To check whether the degradation proceeded through adsorption or photolysis or photocatalysis, we carried out the three sets of reactions: (1) with the catalyst in the dark (2) without the catalyst in light (3) with the catalyst in light, respectively. We observed that there was negligible dye degradation without the catalyst in light and with the catalyst in the dark. The dye degradation was shown with the catalyst in light. The degradation of dye occurred in the presence of light with the catalyst. The comparative study of CuO-1, CuO-2, CuO-3, and CuO-4 revealed that maximum degradation of 84% of dye was observed with the CuO-1 catalyst in the same experimental conditions (Figure 12A). Therefore, we chose the CuO-1
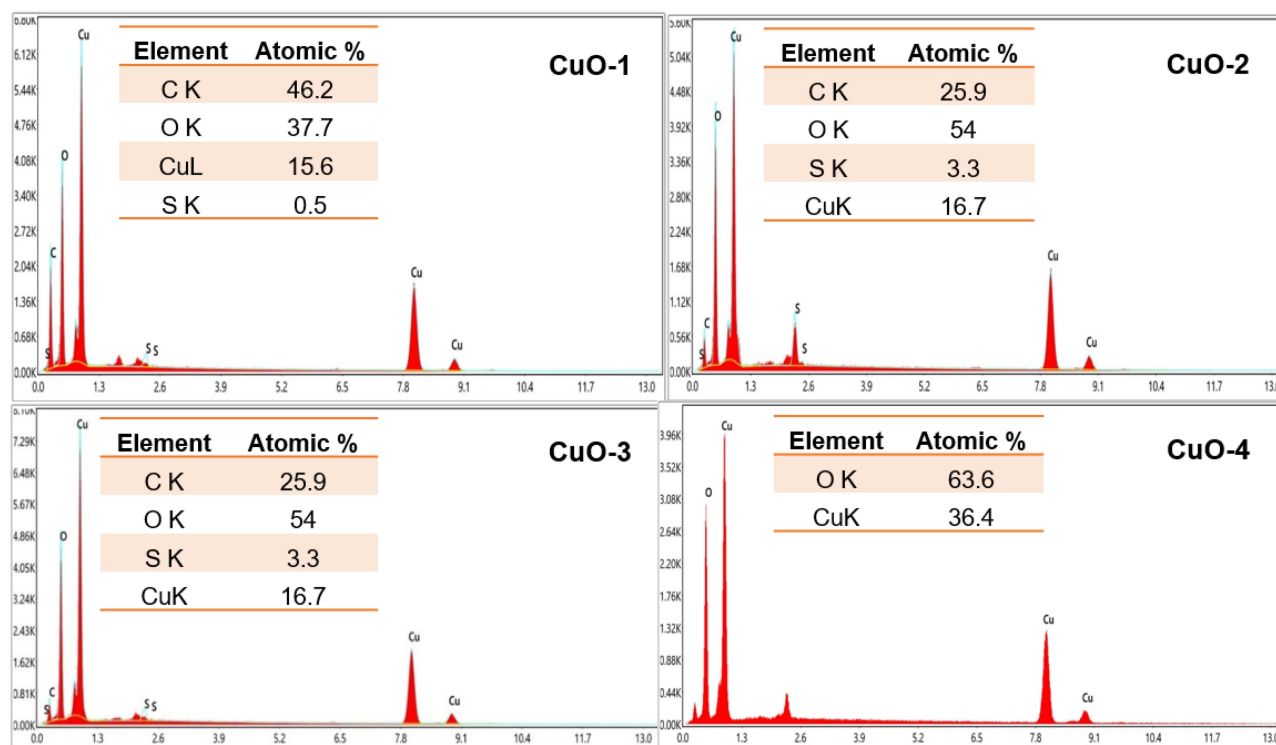
Figure 10 EDS spectra of the biosynthesized CuO NPs (CuO-1, CuO-2, and CuO-3) and chemically synthesized CuO NPs (CuO-4).
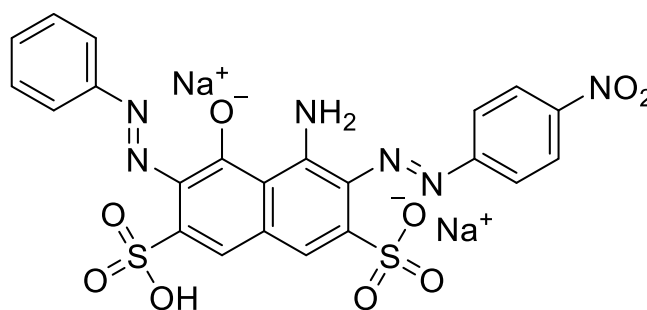

Figure 11 Structure of AB10B dye.

nanocatalyst for further study. Various parameters, like the pH of the solution, the concentration of dye, and the dosage of CuO-1 nanocatalyst, were used for the optimization of reaction parameters.

Effect of pH

As pH is an important factor in the degradation process, an investigation was done using CuO-1 nanocatalyst by changing the pH of the AB10B dye solution by addition of dil. H_2SO_4 or dil. NaOH solution. It is also a noteworthy operational parameter in wastewater treatment. To decide the optimum pH value for the degradation of AB10B dye, the degradation study was conducted over a pH range of 5–9 maintaining other parameters constant. The results are disclosed in Figure 12B. At pH values 5, 6, 7, 8, and 9, the observed degradation percentage was 68.75%, 88.84%, 86.59%, 83.63%, and 81.36%, respectively. The investigation revealed that the pH of the solution significantly altered the photodegradation rate % of AB10B dye. The maximum dye degradation was observed at pH 6 with the degradation efficacy of 88.84%. Therefore, pH 6 was selected for the optimization of other parameters.
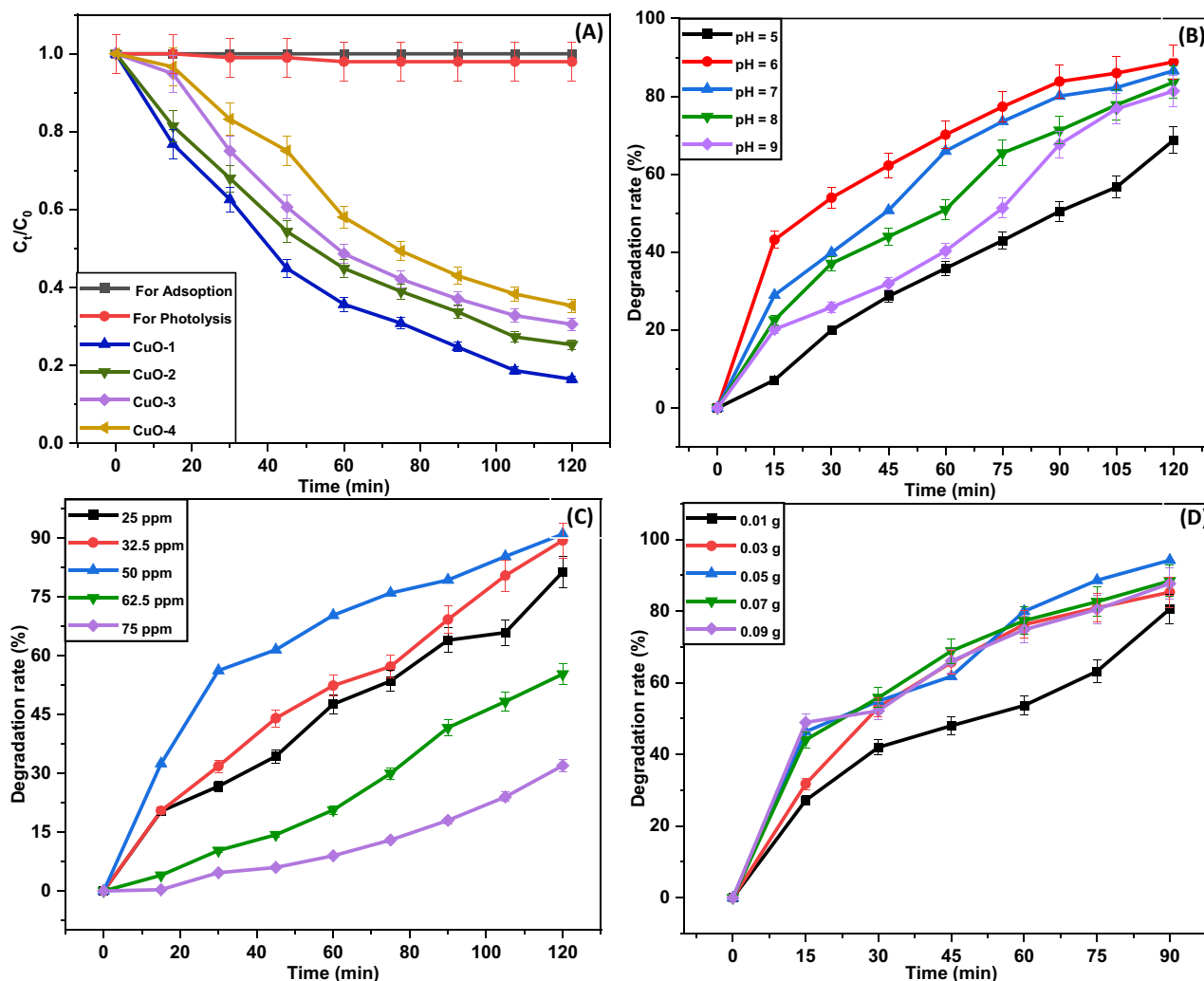
Figure 12 (**A**) Relative examinations of the decay rate of the AB10B dye using the catalyst in the dark, without catalyst in light, CuO-1 (in light), CuO-2 (in light), CuO-3 (in light), and CuO-4 (in light); Experimental study of Effect of (**B**) pH (**C**) dye concentration (**D**) catalyst dosage on the degradation of AB10B dye using CuO-1 catalyst.

Effect of Dye Concentration

To determine the AB10B dye concentration effect on photocatalytic activity, we varied it from 25 ppm to 75 ppm by keeping other parameters constant. The results obtained are shown in Figure 12C. As the concentration of the dye increased from 25 ppm to 50 ppm, the percentage of degradation enhanced from 81.39% to 91.03%, and on further increasing the dye concentration to 75 ppm, the percentage degradation diminished excessively and reached 33%. As an outcome, 50 ppm of dye concentration was found to be optimal. At a low dye concentration, the concentration of oxidizing radicals is greater than necessary to breakdown the dye molecules, while at a high dye concentration, the available oxidizing radicals are insufficient to degrade all the dye molecules. Additionally, as the dye concentration increased further, the dye's colour became more intense and prevented the light penetration to the catalyst surface.

Effect of Catalyst Dosage

The influence of catalyst dosage on the degradation of AB10B dye was investigated by changing the catalyst loading from 0.01 g to 0.09 g at optimized pH 6 and dye concentration of 50 ppm (Figure 12D). Upon increasing the catalyst dosage from 0.01 g to 0.05 g, the degradation capacity improved from 80.56% to 94.19%. However, further increments in the catalyst dosage led to a decrease in the degradation percentage, reaching 87.64%. The increased surface area and the availability of more adsorption sites for the AB10B dye are the key reasons for the upsurge in the dye degradation

Table 6 Optimized Reaction Conditions for the Degradation of AB10B Dye by CuO-1 Nanocatalyst

S. No.	Optimized Parameters	Optimized Values
1.	pH	6
2.	Concentration of dye	50 ppm
3.	Catalyst dose	0.05 g

ability with increasing amounts of the catalyst. The saturation of all the adsorbent's possible active sites may explain why there is no discernible change in the degradation rate after the optimal dosage. Hence, 0.05 g was a suitable quantity of CuO-1 nanocatalyst for the maximum degradation of the dye. The ideal conditions for the degradation of the AB10B dye by the CuO-1 photocatalyst under visible light are shown in Table 6.

The recyclability of the catalyst improves the economic profile and environmental impact of the catalyst. To recover the catalyst, the dye solution with the catalyst was centrifuged and washed 3 times with DI water. After drying, the catalyst was used for further study. Here, the catalyst was recycled and reused successfully for up to 5 cycles and showed minimum loss of catalytic activity (Figure 13). Figure 14 represents that photocatalytic degradation of AB10B was fitted to the Langmuir-Hinshelwood model by
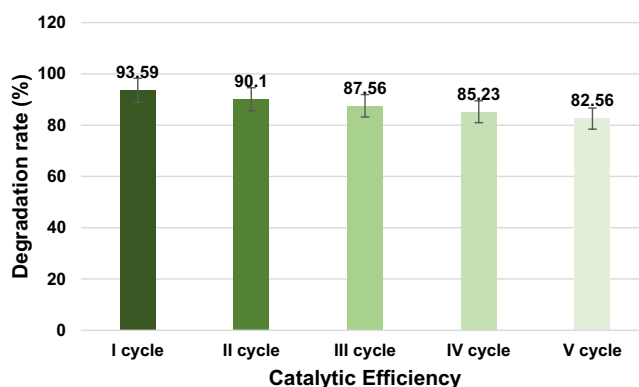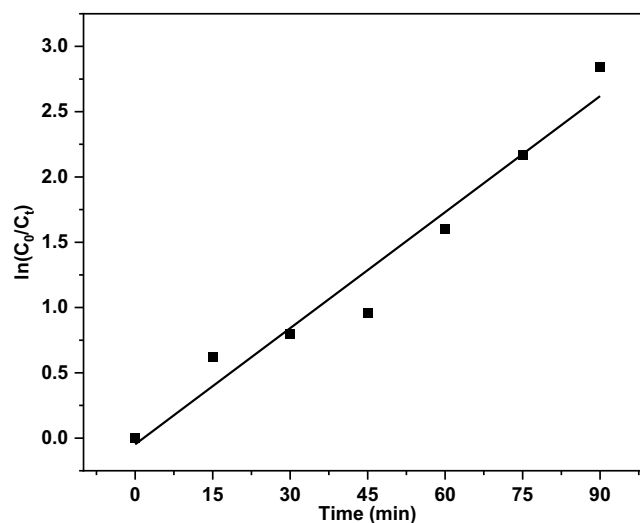

Figure 13 Graphical representation of CuO-1 reusability.

Figure 14 Kinetic investigation of the photocatalytic degradation of AB10B dye after optimizing all the parameters at pH = 6, the concentration of dye = 50 ppm, and the dose of catalyst = 0.05 g.

Table 7 Comparative Photodegradation Studies of AB10B Using Various Nanocatalysts

S. No.	Nanocatalysts	Light Source	Initial Concentration of Dye (ppm)	Catalyst Dosage (mg)	pH	Time (Min)	Removal Percentage (%)	References
1.	TiO_2 NPs	UV	100	200	–	150	30%	[75]
2.	ZnO/Al_2O_3 (1:1)	Solar	1000	150	>7	240	98%	[76]
3.	CeO_2 NPs	UV	–	300	3	155	70.1%	[77]
4.	RGO-NiS	Visible	10	10	7	120	99%	[78]
5.	Zn/Mg co-doped TiO_2	Visible	10	100	3	20	99%	[79]
6.	**CuO NPs**	Visible	50	50	6	90	94%	**This work**

Abbreviation: RGO, Reduced-graphene oxide.

plotting $In(C_0/C_t)$ against irradiation time (t) to get a straight line with linear regression coefficient (R^2) equal to 0.9604. The pseudo rate constant (k) calculated from the slope was 0.0296 min^{-1}.

Table 7 shows the comparison of some representative examples of photocatalytic degradation of AB10B dye using different nanocatalysts. The initial concentration of AB10B dye, catalyst dosage, pH, time, and degradation percentage of AB10B dye were compared with various nanocatalysts.

Scavenging Activity

To understand the major contribution of each primary reactive species, i.e., electrons (e−), ˙OH radicals, and superoxide anion radicals ($O_2^{˙-}$), in the photodegradation process, a series of scavenging experiments were carried out during the photocatalytic process. $K_2Cr_2O_7$, isopropyl alcohol (IPA), and benzoquinone (BQ) were chosen as the scavenging reagents for electrons (e−), ˙OH radicals, and superoxide anion radicals ($O_2^{˙-}$), respectively (Figure 15). The addition of $K_2Cr_2O_7$ slightly decreased the dilapidation of the AB10B dye, which disclosed that electrons (e−) are not involved in the photodegradation of AB10B dye. Furthermore, the photodegradation reaction performed in the presence of IPA and BQ significantly suppressed the photodegradation efficacy from 93.59% to 67.81% and 64.55% after 120 min of reaction, respectively, indicating that the ˙OH radical and subsequent $O_2^{˙-}$ were major active species in the degradation of AB10B dye under visible light irradiation.
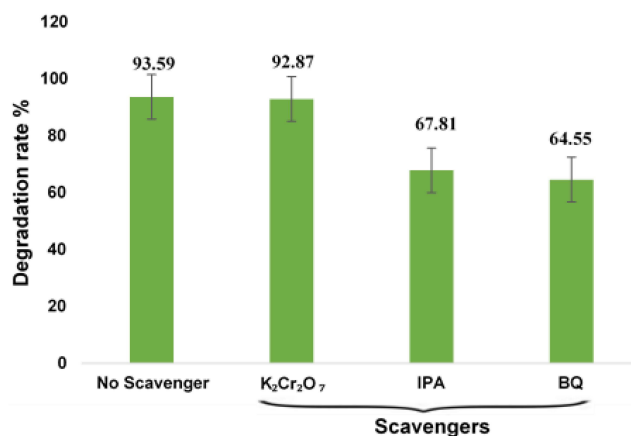

Figure 15 Examining the effect of distinct scavengers on the degradation of AB10B using CuO-1.

Mechanism of Photocatalytic Degradation

Figure 16 depicts the mechanism that constitutes the photocatalytic performance. The photocatalyst works on the principle of the transition of photoexcited electrons from the VB to the CB. These migrated electrons (e−) leave holes (h+) in the VB. When the energy of absorbed light is equal to or greater than the band gap energy of CuO NPs, then the excitation of the electron occurs.[80] These electrons and holes can follow one of two paths: either recombine and create intense fluorescence emissions or seek a pathway to the material's surface and interact with water and oxygen molecules to obtain different reactive oxygen species (ROS). The band gap (2.40 eV) of CuO-1 was the lowest among all biosynthesized CuO NPs and showed the best photocatalytic activity among them. ROS generation depends on two factors: (1) electronic structure and (2) the redox potential of various ROS species. The electronic structure of CuO NPs was described using the band gap (E_g) value, which is 2.40 eV for CuO-1. Equations (8) and (9) were used to calculate the conduction band edge minima (E_{CB}) and valence band maxima (E_{VB}) of the CuO-1 photocatalyst, as shown below.[81]

$$E_{CB} = \chi - 0.5E_g + E_e \qquad (8)$$

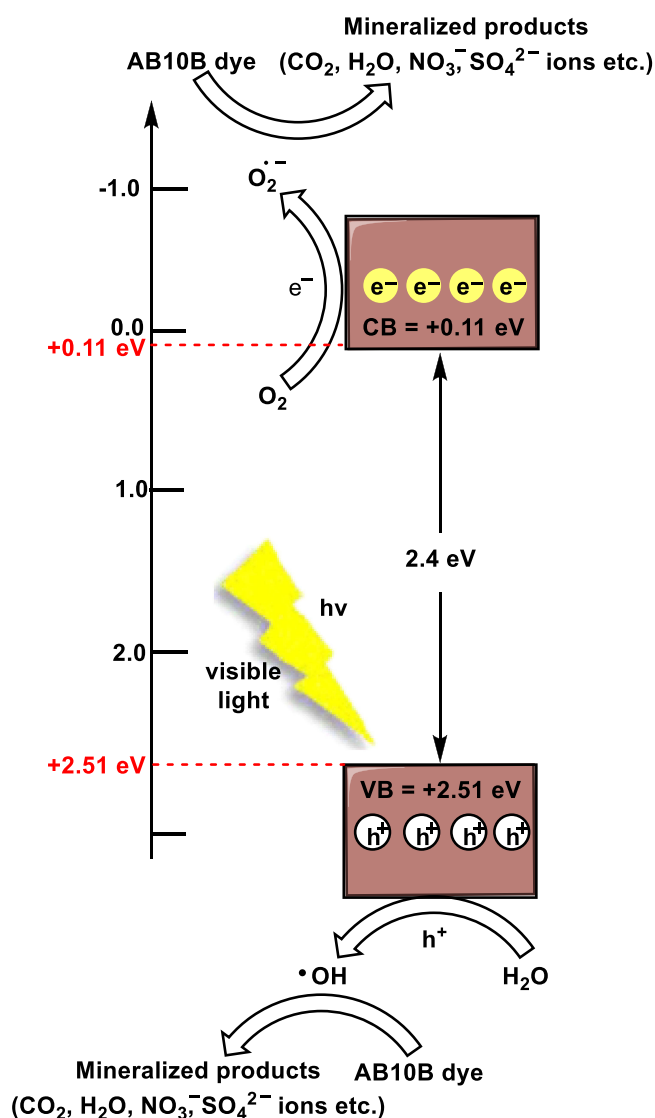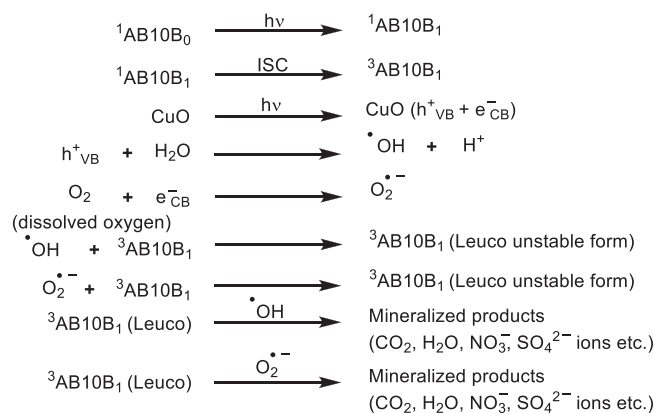$$E_{VB} = E_{CB} + E_g \qquad (9)$$

Figure 16 A plausible mechanism of degradation of AB10B dye using CuO-1 nano photocatalyst.

Scheme 1 Mechanism pathway of the degradation of AB10B dye.

$$\chi = \left[\chi(A)^a . \chi(A)^b\right]^{1/(a + b)} \tag{10}$$

Where E_{CB}, E_g, E_e, and E_{VB} denote the band edge potential of the conduction band (CB), the band gap of the CuO-1 nanocatalyst (2.40 eV), the energy of the free electron (−4.50 eV) on the normal hydrogen electrode (NHE) scale,[82] and band edge potential of valance band (VB), respectively. The χ is calculated using equation (10), the geometric mean of electronegativity of constituent atoms, i.e., copper (Cu) and oxygen (O).[83] Copper (Cu) and oxygen (O) were assigned electronegativity values of 4.48 and 7.54 eV, respectively.[84] The calculated band edge potential of the CB (E_{CB}) and VB (E_{VB}) were 0.11 eV and 2.51 eV, respectively. Figure 16 and Scheme 1 show the plausible mechanism of photocatalytic degradation of dye.

Water Analysis Parameters Before and After Photocatalytic Activity

These biosynthesized CuO NPs are eco-friendly as we analyzed the water sample before and after photocatalytic activity to degrade the dye and check its impact on the environment. Various water quality parameters were used, such as pH, conductance, total dissolved solids (TDS), chemical oxygen demand (COD), and dissolved oxygen (DO), for the assessment of the successful treatment of wastewater containing AB10B dye. Table 8 contains the various water analysis parameters evaluated before and after photocatalytic activity. The data study disclosed the efficiency of biosynthesized CuO NPs to diminish the COD levels from 240 mgL^{-1} to 42 mgL^{-1} with a removal percentage of 82.5%. The high reduction of COD values reflects the potency of CuO NPs to degrade AB10B dye.[85,86] Initially, these dyes were found in complex states, and after degradation, these dyes converted into mineralized ions and, therefore, responsible for the slight increment in TDS and conductance.[87] After degradation, the pH of the solution reached to neutral and made it suitable for aquatic plants and animals. The results displayed that after degradation the quality of water was upgraded.

Table 8 Water Analysis Parameters Before and After Degradation of AB10B Dye by CuO NPs

S. No.	Parameter (Unit)	Before Photocatalytic Treatment	After Photocatalytic Treatment by CuO NPs
1.	pH	7.6	7.1
2.	Conductance (µS)	44.77	119.40
3.	TDS (ppm)	30	90
4.	COD (mg/L)	240	42
5.	DO (ppm)	0.2	6.4

Antimicrobial Activity of Synthesized CuO NPs

Minimum Inhibitory Concentration (MIC) Value of CuO NPs

An antibacterial assay using a well-cut method was used to determine the MIC of biosynthesized and chemically synthesized CuO NPs against two test pathogens- *Staphylococcus aureus* (*S. aureus*) and *Pseudomonas aeruginosa* (*P. aeruginosa*).[88] The algal biosynthesized CuO NPs were denoted as CuO-1, CuO-2, and CuO-3 and chemically synthesized CuO NPs were denoted as CuO-4. The MIC values for both test pathogens, *S. aureus* and *P. aeruginosa* at various CuO NPs concentrations were shown in Tables 9 and 10, respectively. For better understanding, we have also plotted the bar graph (Figure 17) of MIC value (μg/mL) for different concentrations of CuO NPs and antibiotic drug (ofloxacin) against *S. aureus* and *P. aeruginosa*. The lowest inhibitory concentration of all CuO NPs was 75 μL and 150 μL for *S. aureus* and *P. aeruginosa*, respectively. The size of the zone of inhibition (ZOI) was gradually increased due to the increase in concentration (75, 100, 150, and 200 μL) of CuO NPs, loaded on agar well, and it also varied widely because of biologically (CuO-1, CuO-2, and CuO-3) and chemically (CuO-4) synthesized CuO NPs. The chemically synthesized CuO NPs (CuO-4) exhibited the lowest ZOI at all concentrations of CuO NPs for *S. aureus*, as shown in Table 9. The MIC value was highest, i.e., 150 μL for the chemically synthesized CuO NPs (CuO-4) against *P. aeruginosa*. In contrast, CuO-1 (algal-mediated CuO NPs) showed the lowest MIC value of 75 μL. The MIC values reported in this literature were somewhat better than Parsaee and co-authors[43] and Ahangar et al[89] findings because we used 0.5 mg/mL concentration of CuO NPs for antibacterial assay, while the above-mentioned reports used a higher concentration (5 mg/mL) of CuO NPs. Therefore, we can conclude that a ten times lower concentration of synthesized CuO NPs provided noticeably stronger antibacterial activity than previously reported findings.

Antibacterial Assay Using Disc Diffusion Method.

The standard Kirby-Bauer disc diffusion method was utilized to investigate the antibacterial activity of CuO NPs against test microorganisms. The Ofloxacin and DI water were used as positive and negative controls for the antibacterial assay, respectively. All four synthesized CuO NPs exhibited a higher ZOI (mm) against *S. aureus*, i.e., CuO-1 (22 mm), CuO-2 (19 mm), CuO-3 (19 mm), CuO-4 (14 mm), and positive control/antibiotic (14 mm). Surprisingly, CuO-1 exhibited

Table 9 MIC of Biosynthesized and Chemically Synthesized CuO NPs Against *S. aureus*

		ZOI (mm)						
S. No.	**Sample Name**	**Concentration of Nanoparticles (μL)**					**Positive Control (μL)**	**Negative Control (μL)**
		50	**75**	**100**	**150**	**200**		
1.	CuO-1	Nil	18 mm	19 mm	20 mm	22 mm	14 mm	NA
2.	CuO-2	Nil	15 mm	15 mm	16 mm	17 mm	15 mm	NA
3.	CuO-3	Nil	17 mm	17 mm	18 mm	19 mm	14 mm	NA
4.	CuO-4	Nil	9 mm	10 mm	12 mm	12 mm	16 mm	NA

Table 10 MIC of Biosynthesized and Chemically Synthesized CuO NPs Against *P. aeruginosa*

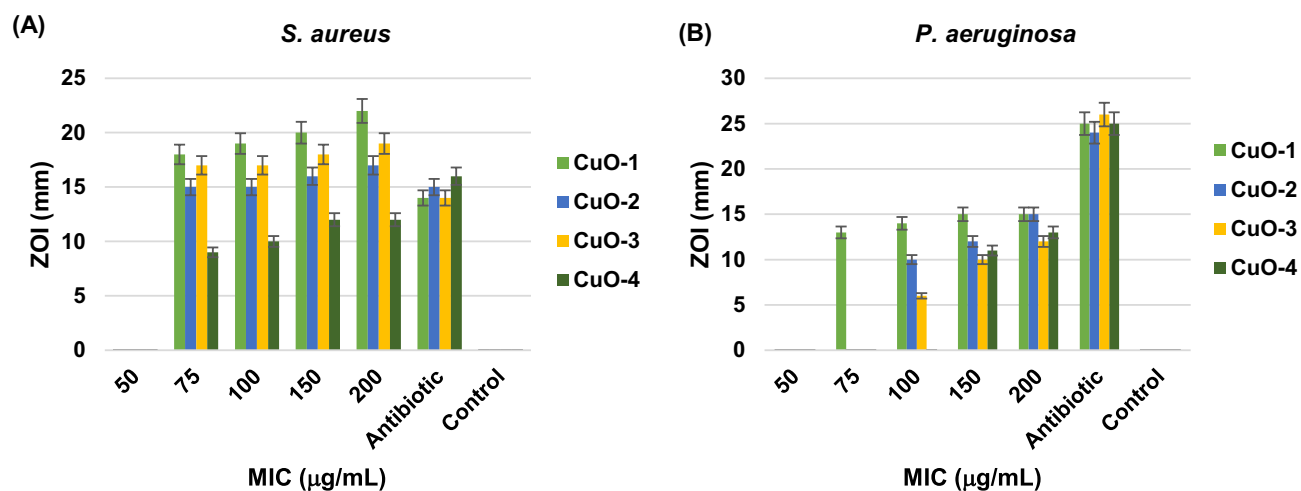|		ZOI (mm)						
S. No.	**Sample name**	**Concentration of Nanoparticles (μL)**					**Positive Control (μL)**	**Negative Control (μL)**
		50	**75**	**100**	**150**	**200**		
1.	CuO-1	Nil	13mm	14 mm	15 mm	15 mm	25 mm	NA
2.	CuO-2	Nil	Nil	10 mm	12 mm	15 mm	24 mm	NA
3.	CuO-3	Nil	Nil	6 mm	10 mm	12 mm	26 mm	NA
4.	CuO-4	Nil	Nil	Nil	11 mm	13 mm	25 mm	NA

Figure 17 Bar graph showing MIC value (µg/mL) for different concentrations of CuO NPs, antibiotics/positive control, and negative control against (**A**) *S. aureus* and (**B**) *P. aeruginosa* bacterial strains.

higher antibacterial activity with a ZOI value of 22 mm than positive control with a ZOI value of 14 mm against *S. aureus*. For *P. aeruginosa*, the ZOI value was, CuO-1 (17 mm), CuO-2 (16 mm), CuO-3 (14 mm), CuO-4 (13 mm), and positive control/antibiotic (25 mm). When compared to chemically synthesized CuO NPs (CuO-4), the biologically synthesized CuO NPs (CuO-1, CuO-2, and CuO-3) have higher ZOI, as represented in Figure 18, and associated data values are given in Table 11. Abboud et al reported the 16 mm ZOI value for *S. aureus* bacteria.[42] Ahangar and co-workers examined the antibacterial activity of CuO NPs. The ZOI value reported by them were 12 mm for *S. aureus* and 10 mm for *P. aeruginosa* at the 5 mg/mL concentration of CuO NPs.[89] Table 12 represents a comparative analysis of the antibacterial activity of CuO NPs synthesized previously using algal extract. From the current findings, we conclude that the test pathogens were strongly impacted by the antagonistic activity of green algal-mediated CuO NPs in contrast to chemically synthesized CuO NPs.

Effect of Size and Shape on Antibacterial Activity of CuO NPs.

The size of the NPs is an essential factor in the antibacterial assay. Among all the biosynthesized NPs, CuO NPs synthesized from the 15 mL algal extract (CuO-1) showed superior activity for both tested pathogens due to their lowest size, 7.62 nm, along the maximum intensity plane (111). For *S. aureus*, the ZOI of CuO-1 (22 mm) was even higher than
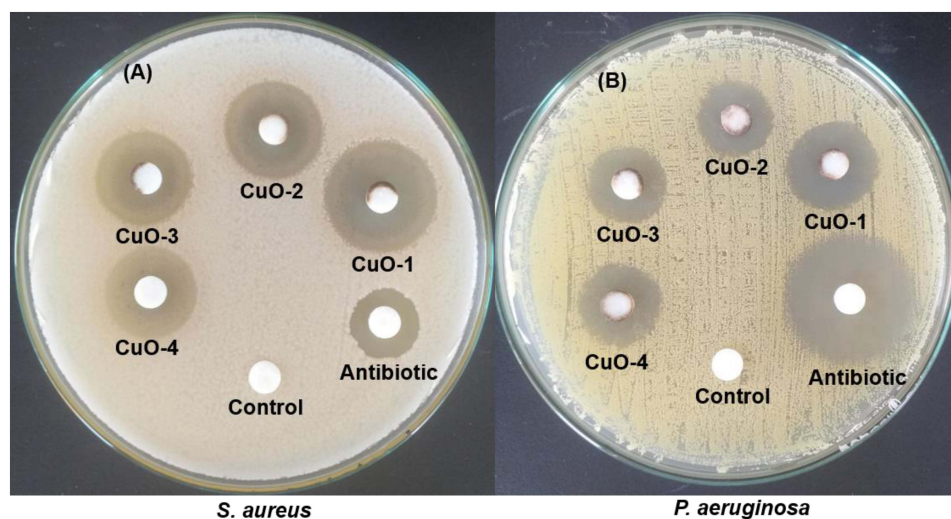

Figure 18 Antagonistic activity of biosynthesized CuO NPs (CuO-1, CuO-2, CuO-3), chemically synthesized CuO NPs (CuO-4), antibiotic/positive control, and negative control against test pathogens (**A**) *S. aureus* and (**B**) *P. aeruginosa* utilizing the disc diffusion method.

Table 11 Antibacterial Assay Showing ZOI (Mm) of the Synthesized CuO NPs Against *S. aureus* and *P. aeruginosa*

		ZOI (mm)					
S. No.	**Target bacteria**	**CuO-1 (µL)**	**CuO-2 (µL)**	**CuO-3 (µL)**	**CuO-4 (µL)**	**Positive Control (µL)**	**Negative Control (µL)**
1.	*S. aureus*	**22 mm**	19 mm	19 mm	14 mm	14 mm	NIL
2.	*P. aeruginosa*	**17 mm**	16 mm	15 mm	13 mm	25 mm	NIL

Notes: The bold value represents the highest ZOI observed against both *S. aureus* and *P. aeruginosa* among the various CuO NPs tested.

Table 12 Comparative Study of Antibacterial Activity of Some Previously Reported Algae-Mediated CuO NPs

S. No.	**Nanoparticles (NPs)**	**Algal Species**	**Size (nm)**	**Target Bacteria**	**ZOI (mm)**	**References**
1.	CuO NPs	*Bifurcaria bifurcata*	5–45	*E. aerogenes* and *S. aureus*	14 and 16	[42]
2.	CuO NPs	*Sargassum polycystum*	–	*P. aeruginosa* and *Shigella dysenteriae*	15 ± 0.5 and 6 ± 0.5	[28]
3.	CuO NPs	*Cystoseira trinodis*	7.43	*E. faecalis, E. coli, S. typhimurium, B. subtilis, S. aureus*, and *S. faecalis*, respectively	16.57, 18.79, 12.62, 12.76, 17.48, and 13.27, respectively	[43]
4.	CuO NPs	*Anabaena cylindrica*	3.6	*E. coli*	4.5 ± 0.7	[44]
5.	CuO NPs	*Sargassum longifolium*	40–60	*Serratia marcescens, Vibrio parahemolyticus*, and *Aeromonas hydrophila*, respectively	14 ± 0.34,16 ± 0.18, and 17 ± 1.12, respectively	[46]
6.	**CuO NPs (CuO-1)**	*Coelastrella terrestris*	5.81–13.54	*S. aureus* and *P. aeruginosa*	22 and 17	**This work**

Abbreviations: *E. aerogenes*, Klebsiella aerogenes; *E. faecalis*, Enterococcus faecalis; *E. coli*, Escherichia coli; *S. typhimurium*, Salmonella typhimurium; *B. subtilis*, Bacillus subtilis; *S. faecalis*, Streptococcus faecalis.

the positive control of ofloxacin (14 mm), as shown in Figure 18. For *P. aeruginosa*, CuO-1 also showed the best antibacterial activity from all synthesized NPs due to its small size. Within the CuO NPs, the lowest antibacterial activity was observed by chemically synthesized CuO NPs (CuO-4) against both tested pathogens i.e., 14 mm ZOI value for *S. aureus* and 13 mm ZOI value for *P. aeruginosa*. The reason behind the lowest antibacterial activity of chemically synthesized CuO NPs was a consequence of their large crystallite size of 20.38 nm along the maximum intensity plane (−111) in contrast to biologically synthesized CuO NPs, as mentioned in Table 3. The results indicated that flattened rice-like structures CuO-1 NPs exhibited higher antibacterial activity than flower petal-like structures CuO-3 NPs.

From the results, it was inferred that *Coelastrella terrestris* algal-mediated CuO NPs were more efficient on *S. aureus* (Gram-positive) compared to *P. aeruginosa* (Gram-negative) bacteria. Our findings are consistent with Azam et al[90] and Suresh and co-authors' results,[91] who demonstrated that the action of CuO NPs was more prominent against Gram-positive bacteria than Gram-negative bacteria. The difference in the activity can be ascribed to the difference in the outer membrane of the Gram-positive and Gram-negative bacterial strains. The cell wall of Gram-positive bacteria (*S. aureus*) is made up of a thick peptidoglycan layer which induces resistance against the release of Cu^{+2} ions.[91–93] On the contrary, the cell membrane of Gram-negative bacteria had a thin peptidoglycan layer along with lipopolysaccharides surrounding them which could be damaged as a consequence of the Cu^{+2} ions penetration.[92]
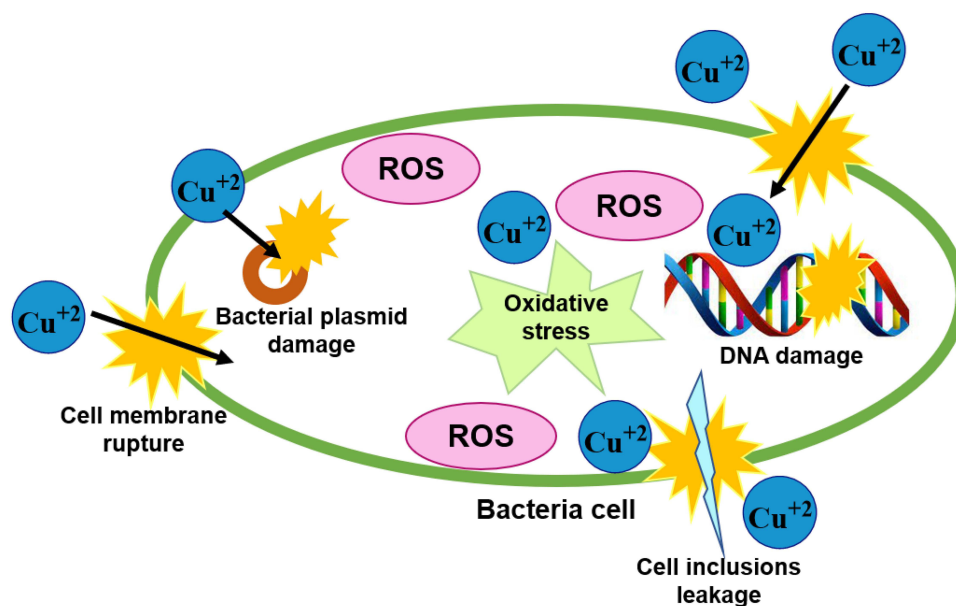
Figure 19 A plausible antibacterial mechanism of synthesized CuO NPs.

The predominant bactericidal mechanism of CuO NPs mainly involves the generation of ROS, like superoxide anion radicals ($O_2^{\cdot-}$) and hydroxyl radicals ($^{\cdot}OH$). These ROS trigger oxidative stress and destroy the cellular membrane, which harms various macromolecules, cell walls, DNA, and bacterial plasmids, and even directs to cell death.[94,95] Figure 19 shows the schematic illustration of a plausible antibacterial mechanism of CuO NPs.

Conclusion

The present study illustrates the facile, straightforward, eco-friendly, and practical approach for synthesizing CuO NPs via *Coelastrella terrestris* algal extract. The structural, morphological, and optical properties of the synthesized NPs were investigated in detail using XRD, FTIR, UV-Vis, DLS, FE-SEM, and EDS. The XRD study revealed that particle size decreases along the (110) plane and increases along the (111) plane with the enhancement of the algal extract volume. The FTIR analysis disclosed that the phytochemical molecules of algal extract were responsible for the function of reduction, stabilization, and capping in the synthesis of CuO NPs. The FE-SEM images showed that enrichment of the algal extract during the nucleation process clubbed the flattened rice-like structures to flower petals. The synthesized CuO-1 NPs with lowest band gap value (2.40 eV) were shown to be effective in degrading AB10B dye, with a degradation efficiency of 94.19% being observed at optimal conditions. The antibacterial activity findings inferred that *Coelastrella terrestris* algal-mediated CuO NPs were more effective on *S. aureus* (Gram-positive) with a ZOI value of 22 mm compared to *P. aeruginosa* (Gram-negative) with a ZOI value of 17 mm bacterial strain. In summary, an eco-friendly *Coelastrella terrestris*-mediated biosynthesis of CuO NPs can be a potential contender for removing the contaminants from wastewater. Subsequent investigations should prioritize assessing the applicability of CuO NPs in extensive wastewater and bacterial treatment systems with their potential impacts on the ecosystem.

Associated Content

All experimental details are explained in the Supplementary Material 1.

Data Sharing Statement

All data generated or analyzed during this study are included in this published article. Additional data can be provided upon request from the corresponding author.

Acknowledgments

Author Contributions

All authors made a significant contribution to the work reported, whether that is in the conception, study design, execution, acquisition of data, analysis and interpretation, or in all these areas; took part in drafting, revising or critically reviewing the article; gave final approval of the version to be published; have agreed on the journal to which the article has been submitted; and agree to be accountable for all aspects of the work.

Funding

Disclosure

The authors have no competing interests to declare that are relevant to the content of this article.

References

1. Wijesinghe U, Thiripuranathar G, Iqbal H, Menaa F. Biomimetic synthesis, characterization, and evaluation of fluorescence resonance energy transfer, photoluminescence, and photocatalytic activity of zinc oxide nanoparticles. *Sustainability.* 2021;13(4):2004. doi:10.3390/su13042004

2. Aravind M, Amalanathan M, Mary M. Synthesis of TiO2 nanoparticles by chemical and green synthesis methods and their multifaceted properties. *SN Appl Sci.* 2021;3(4):1–10. doi:10.1007/s42452-021-04281-5

3. Khandelwal M, Kumawat A, Misra KP, Khangarot RK. Efficient antibacterial activity in copper oxide nanoparticles biosynthesized via Jasminum sambac flower extract. *Part Sci Technol.* 2022;2:1–13.

4. Jabbar A, Abbas A, Assad N, et al. A highly selective Hg2+ colorimetric sensor and antimicrobial agent based on green synthesized silver nanoparticles using Equisetum diffusum extract. *RSC Adv.* 2023;13(41):28666–28675. doi:10.1039/D3RA05070J

5. Siddique AB, Amr D, Abbas A, et al. Synthesis of hydroxyethylcellulose phthalate-modified silver nanoparticles and their multifunctional applications as an efficient antibacterial, photocatalytic and mercury-selective sensing agent. *Int J Biol Macromol.* 2024;256:128009. doi:10.1016/j.ijbiomac.2023.128009

6. Ejaz A, Mamtaz Z, Yasmin I, et al. Cyperus scariosus extract based greenly synthesized gold nanoparticles as colorimetric nanoprobe for Ni2+ detection and as antibacterial and photocatalytic agent. *J Mol Liq.* 2024;393:123622. doi:10.1016/j.molliq.2023.123622

7. Saied E, Salem SS, Al-Askar AA, Elkady FM, Arishi AA, Hashem AH. Mycosynthesis of hematite (α-Fe2O3) nanoparticles using Aspergillus Niger and their antimicrobial and photocatalytic activities. *Bioengineering.* 2022;9(8):397. doi:10.3390/bioengineering9080397

8. Salem SS, Hammad EN, Mohamed AA, El-Dougdoug W. A comprehensive review of nanomaterials: types, synthesis, characterization, and applications. *Biointerface Res Appl Chem.* 2022;13(1):41.

9. Salem SS, Fouda A. Green synthesis of metallic nanoparticles and their prospective biotechnological applications: an overview. *Biol Trace Elem Res.* 2021;199(1):344–370. doi:10.1007/s12011-020-02138-3

10. Dezfuli AAZ, Abu-Elghait M, Salem SS. Recent insights into nanotechnology in colorectal cancer. *Appl Biochem Biotechnol.* 2023;2:1–15.

11. Salem SS. A mini review on green nanotechnology and its development in biological effects. *Arch Microbiol.* 2023;205(4):128. doi:10.1007/s00203-023-03467-2

12. Hussein AS, Hashem AH, Salem SS. Mitigation of the hyperglycemic effect of streptozotocin-induced diabetes albino rats using biosynthesized copper oxide nanoparticles. *Biomole Conc.* 2023;14(1). doi:10.1515/bmc-2022-0037

13. Mohamed AA, Abu-Elghait M, Ahmed NE, Salem SS. Eco-friendly mycogenic synthesis of ZnO and CuO nanoparticles for in vitro antibacterial, antibiofilm, and antifungal applications. *Biol Trace Elem Res.* 2021;199(7):2788–2799. doi:10.1007/s12011-020-02369-4

14. Fouda A, Salem SS, Wassel AR, Hamza MF, Shaheen TI. Optimization of green biosynthesized visible light active CuO/ZnO nano-photocatalysts for the degradation of organic methylene blue dye. *Heliyon.* 2020;6(9):e04896. doi:10.1016/j.heliyon.2020.e04896

15. Cuong HN, Pansambal S, Ghotekar S, et al. New frontiers in the plant extract mediated biosynthesis of copper oxide (CuO) nanoparticles and their potential applications: a review. *Environ Res.* 2022;203:111858. doi:10.1016/j.envres.2021.111858

16. Shaheen TI, Fouda A, Salem SS. Integration of cotton fabrics with biosynthesized CuO nanoparticles for bactericidal activity in the terms of their cytotoxicity assessment. *Ind Eng Chem Res.* 2021;60(4):1553–1563. doi:10.1021/acs.iecr.0c04880

17. Chaudhary S, Rohilla D, Umar A, Kaur N, Shanavas A. Synthesis and characterizations of luminescent copper oxide nanoparticles: toxicological profiling and sensing applications. *Ceram Int*. 2019;45(12):15025–15035. doi:10.1016/j.ceramint.2019.04.239

18. Nasibulin AG, Ahonen PP, Richard O, Kauppinen EI, Altman IS. Copper and copper oxide nanoparticle formation by chemical vapor nucleation from copper (II) acetylacetonate. *J Nanopart Res*. 2001;3(5):383–398. doi:10.1023/A:1012508407420

19. Khatoon UT, Velidandi A, Nageswara Rao GVS. Copper oxide nanoparticles: synthesis via chemical reduction, characterization, antibacterial activity, and possible mechanism involved. *Inorg Chem Commun*. 2023;149:110372. doi:10.1016/j.inoche.2022.110372

20. Suzuki K, Tanaka N, Ando A, Takagi H. Size-selected copper oxide nanoparticles synthesized by laser ablation. *J Nanopart Res*. 2012;14(5):863. doi:10.1007/s11051-012-0863-z

21. Thanoon HK, Hubeatir KA, Al-Amiery AA. Synthesis of copper oxide nanoparticles via sol-gel method. *Int J Res Engine Innovat*. 2017;1 (4):43–45.

22. Khayati G, Nourafkan E, Karimi G, Moradgholi J. Synthesis of cuprous oxide nanoparticles by mechanochemical oxidation of copper in high planetary energy ball mill. *Adv Powder Technol*. 2013;24(1):301–305. doi:10.1016/j.apt.2012.07.006

23. Cattaruzza E, Battaglin G, Canton P, Sada C. Some structural and optical properties of copper and copper oxide nanoparticles in silica films formed by co-deposition of copper and silica. *J Non Crystalline Solids*. 2005;351(21–23):1932–1936. doi:10.1016/j.jnoncrysol.2005.04.041

24. Liu P, Li Z, Cai W, Fang M, Luo X. Fabrication of cuprous oxide nanoparticles by laser ablation in PVP aqueous solution. *RSC Adv*. 2011;1 (5):847–851. doi:10.1039/c1ra00261a

25. Chan GH, Zhao J, Hicks EM, Schatz GC, Van Duyne RP. Plasmonic properties of copper nanoparticles fabricated by nanosphere lithography. *Nano Lett*. 2007;7(7):1947–1952. doi:10.1021/nl070648a

26. Khatoon UT, Mohan Mantravadi K, Nageswara Rao G. Strategies to synthesise copper oxide nanoparticles and their bio applications–a review. *Mater Sci Technol*. 2018;34(18):2214–2222. doi:10.1080/02670836.2018.1482600

27. Singh J, Kumar V, Kim KH, Rawat M. Biogenic synthesis of copper oxide nanoparticles using plant extract and its prodigious potential for photocatalytic degradation of dyes. *Environ Res*. 2019;177:108569. doi:10.1016/j.envres.2019.108569

28. Ramaswamy SVP, Narendhran S, Sivaraj R. Potentiating effect of ecofriendly synthesis of copper oxide nanoparticles using brown alga: antimicrobial and anticancer activities. *Bull Mater Sci*. 2016;39(2):361–364. doi:10.1007/s12034-016-1173-3

29. Hassan SED, Fouda A, Radwan AA, et al. Endophytic actinomycetes Streptomyces spp mediated biosynthesis of copper oxide nanoparticles as a promising tool for biotechnological applications. *J Biol Inorg Chem*. 2019;24(3):377–393. doi:10.1007/s00775-019-01654-5

30. Mani VM, Kalaivani S, Sabarathinam S, et al. Copper oxide nanoparticles synthesized from an endophytic fungus Aspergillus terreus: bioactivity and anti-cancer evaluations. *Environ Res*. 2021;201:111502. doi:10.1016/j.envres.2021.111502

31. Nzilu DM, Madivoli ES, Makhanu DS, Wanakai SI, Kiprono GK, Kareru PG. Green synthesis of copper oxide nanoparticles and its efficiency in degradation of rifampicin antibiotic. *Sci Rep*. 2023;13(1):14030. doi:10.1038/s41598-023-41119-z

32. Shehabeldine AM, Amin BH, Hagras FA, et al. Potential antimicrobial and antibiofilm properties of copper oxide nanoparticles: time-kill kinetic essay and ultrastructure of pathogenic bacterial cells. *Appl Biochem Biotechnol*. 2023;195(1):467–485. doi:10.1007/s12010-022-04120-2

33. Badawy AA, Abdelfattah NAH, Salem SS, Awad MF, Fouda A. Efficacy assessment of biosynthesized copper oxide nanoparticles (CuO-NPs) on stored grain insects and their impacts on morphological and physiological traits of wheat (Triticum aestivum L.) plant. *Biology*. 2021;10(3):233. doi:10.3390/biology10030233

34. Hammad EN, Salem SS, Zohair MM, Mohamed AA, El-Dougdoug W. Purpureocillium lilacinum mediated biosynthesis copper oxide nanoparticles with promising removal of dyes. *Biointerf Res Appl Chem*. 2022;12(2):1397–1404.

35. Chaudhary R, Nawaz K, Khan AK, Hano C, Abbasi BH, Anjum S. An overview of the algae-mediated biosynthesis of nanoparticles and their biomedical applications. *Biomolecules*. 2020;10(11):1498. doi:10.3390/biom10111498

36. Sinha SN, Paul D, Halder N, Sengupta D, Patra SK. Green synthesis of silver nanoparticles using fresh water green alga Pithophora oedogonia (Mont) Wittrock and evaluation of their antibacterial activity. *Appl Nanosci*. 2015;5(6):703–709. doi:10.1007/s13204-014-0366-6

37. Abdel-Aal EI, Haroon AM, Mofeed J. Successive solvent extraction and GC–MS analysis for the evaluation of the phytochemical constituents of the filamentous green alga Spirogyra longata. *Egyptian J Aqua Res*. 2015;41(3):233–246. doi:10.1016/j.ejar.2015.06.001

38. Haq SH, Al-Ruwaished G, Al-Mutlaq MA, et al. Antioxidant, anticancer activity and phytochemical analysis of green algae, Chaetomorpha collected from the Arabian Gulf. *Sci Rep*. 2019;9(1):1–7. doi:10.1038/s41598-019-55309-1

39. Choudhary S, Kumawat G, Khandelwal M, et al. Sustainable phyco-fabrication of silver nanoparticles using Coelastrella terrestris and their multiple downstream applications. *Biocatal Agric Biotechnol*. 2023;53:102854. doi:10.1016/j.bcab.2023.102854

40. Dahoumane SA, Mechouet M, Wijesekera K, et al. Algae-mediated biosynthesis of inorganic nanomaterials as a promising route in nanobiotechnology–a review. *Green Chem*. 2017;19(3):552–587. doi:10.1039/C6GC02346K

41. Akintelu SA, Folorunso AS, Folorunso FA, Oyebamiji AK. Green synthesis of copper oxide nanoparticles for biomedical application and environmental remediation. *Heliyon*. 2020;6(7):e04508. doi:10.1016/j.heliyon.2020.e04508

42. Abboud Y, Saffaj T, Chagraoui A, et al. Biosynthesis, characterization and antimicrobial activity of copper oxide nanoparticles (CONPs) produced using brown alga extract (Bifurcaria bifurcata). *Appl Nanosci*. 2014;4(5):571–576. doi:10.1007/s13204-013-0233-x

43. Gu H, Chen X, Chen F, Zhou X, Parsaee Z. Ultrasound-assisted biosynthesis of CuO-NPs using brown alga Cystoseira trinodis: characterization, photocatalytic AOP, DPPH scavenging and antibacterial investigations. *Ultrason Sonochem*. 2018;41:109–119. doi:10.1016/j.ultsonch.2017.09.006

44. Bhattacharya P, Swarnakar S, Ghosh S, Majumdar S, Banerjee S. Disinfection of drinking water via algae mediated green synthesized copper oxide nanoparticles and its toxicity evaluation. *J Environ Chem Eng*. 2019;7(1):102867. doi:10.1016/j.jece.2018.102867

45. Araya-Castro K, Chao TC, Durán-Vinet B, Cisternas C, Ciudad G, Rubilar O. Green synthesis of copper oxide nanoparticles using protein fractions from an aqueous extract of Brown Algae Macrocystis pyrifera. *Processes*. 2020;9(1):78. doi:10.3390/pr9010078

46. Rajeshkumar S, Nandhini N, Manjunath K, et al. Environment friendly synthesis copper oxide nanoparticles and its antioxidant, antibacterial activities using Seaweed (Sargassum longifolium) extract. *J Mol Struct*. 2021;1242:130724. doi:10.1016/j.molstruc.2021.130724

47. Khandelwal M, Choudhary S, Kumawat A, Misra KP, Rathore DS, Khangarot RK. Asterarcys quadricellulare algae-mediated copper oxide nanoparticles as a robust and recyclable catalyst for the degradation of noxious dyes from wastewater. *RSC Adv*. 2023;13(40):28179–28196. doi:10.1039/D3RA05254K

48. Veisi H, Karmakar B, Tamoradi T, Hemmati S, Hekmati M, Hamelian M. Biosynthesis of CuO nanoparticles using aqueous extract of herbal tea (Stachys Lavandulifolia) flowers and evaluation of its catalytic activity. *Sci Rep*. 2021;11(1):1983. doi:10.1038/s41598-021-81320-6

49. Letchumanan D, Sok SP, Ibrahim S, Nagoor NH, Arshad NM. Plant-based biosynthesis of copper/copper oxide nanoparticles: an update on their applications in biomedicine, mechanisms, and toxicity. *Biomolecules*. 2021;11(4):564. doi:10.3390/biom11040564

50. Asbrink S, Waskowska A. CuO: x-ray single-crystal structure determination at 196 K and room temperature. *J Phys*. 1991;3(42):8173.

51. Langford J, Louer D. High-resolution powder diffraction studies of copper (II) oxide. *J Appl Crystallogr*. 1991;24(2):149–155. doi:10.1107/S0021889890012092

52. Sharma A, Khangarot RK, Misra KP, et al. Band gap reduction and quenching of pd exchange interaction in sol-gel derived Zn (Al, Cu) O nanostructures. *Phys Scr*. 2021;96(7):075803. doi:10.1088/1402-4896/abf8ea

53. Sharma A, Khangarot RK, Kumar N, Chattopadhyay S, Misra KP. Rise in UV and blue emission and reduction of surface roughness due to the presence of Ag and Al in monocrystalline ZnO films grown by sol-gel spin coating. *Mater Technol*. 2020;1–11. doi:10.1080/10667857.2020.1776029

54. Sharma A, Kumawat A, Raput B, et al. *Effect of Heavy Al Doping on Microstructural and Morphological Behavior of ZnO Thin Film Deposited by Sol-Gel Spin Coating*. Vol. 2352. AIP Publishing LLC; 2021:040001.

55. Pellegrino F, Pellutiè L, Sordello F, et al. Influence of agglomeration and aggregation on the photocatalytic activity of TiO2 nanoparticles. *Appl Catal B*. 2017;216:80–87. doi:10.1016/j.apcatb.2017.05.046

56. Saravanakumar K, Mariadoss AVA, Sathiyaseelan A, Wang MH. Synthesis and characterization of nano-chitosan capped gold nanoparticles with multifunctional bioactive properties. *Int J Biol Macromol*. 2020;165:747–757. doi:10.1016/j.ijbiomac.2020.09.177

57. Kashyap M, Samadhiya K, Ghosh A, Anand V, Shirage PM, Bala K. Screening of microalgae for biosynthesis and optimization of Ag/AgCl nano hybrids having antibacterial effect. *RSC Adv*. 2019;9(44):25583–25591. doi:10.1039/C9RA04451E

58. Balashanmugam P, Kalaichelvan PT. Biosynthesis characterization of silver nanoparticles using Cassia roxburghii DC. aqueous extract, and coated on cotton cloth for effective antibacterial activity. *Int j Nanomed*. 2015;10(sup2):87–97. doi:10.2147/IJN.S79984

59. Jadhav MS, Kulkarni S, Raikar P, Barretto DA, Vootla SK, Raikar US. Green biosynthesis of CuO & Ag–CuO nanoparticles from Malus domestica leaf extract and evaluation of antibacterial, antioxidant and DNA cleavage activities. *New J Chem*. 2018;42(1):204–213. doi:10.1039/C7NJ02977B

60. Rajeshkumar S, Malarkodi C, Paulkumar K, Vanaja M, Gnanajobitha G, Annadurai G. Algae mediated green fabrication of silver nanoparticles and examination of its antifungal activity against clinical pathogens. *Int J Met*. 2014;2014:2. doi:10.1155/2014/692643

61. Borah D, Das N, Das N, et al. Alga-mediated facile green synthesis of silver nanoparticles: photophysical, catalytic and antibacterial activity. *Appl Organomet Chem*. 2020;34(5):e5597. doi:10.1002/aoc.5597

62. Thangaraj M, Saravana BP, Thanasekaran J, Joen-Rong S, Manubolu M, Pathakoti K. Phytochemicals of algae, Arthospira platensis (spirulina) Chlorella vulgaris (chlorella) and Azolla pinnata (azolla). *GSC Bio Pharm Sci*. 2022;19(2):023–043. doi:10.30574/gscbps.2022.19.2.0167

63. Benhadria N, Hachemaoui M, Zaoui F, et al. Catalytic reduction of methylene blue dye by copper oxide nanoparticles. *Journal of Cluster Sci*. 2022;33(1):249–260. doi:10.1007/s10876-020-01950-0

64. Selvam K, Albasher G, Alamri O, et al. Enhanced photocatalytic activity of novel Canthium coromandelicum leaves based copper oxide nanoparticles for the degradation of textile dyes. *Environ Res*. 2022;211:113046. doi:10.1016/j.envres.2022.113046

65. Sharma A, Kumawat A, Chattopadhyay S, Khangarot RK, Misra R, Misra KP. Low temperature induced red-shift in violet-blue emission from Zn (Al, Ag) O nanoparticles. *Mater Technol*. 2021;5:1–10.

66. Sharma A, Kumawat A, Chattopadhyay S, et al. Band gap reduction and Zn related defects enhancement in Zn (Al, Ce) O nanoparticles. *Mater Today*. 2022;60:21–25.

67. Misra KP, Shukla R, Srivastava A, Srivastava A. Blueshift in optical band gap in nanocrystalline Zn 1− x Ca x O films deposited by sol-gel method. *Appl Phys Lett*. 2009;95(3):031901. doi:10.1063/1.3184789

68. Shreyash N, Bajpai S, Khan MA, Vijay Y, Tiwary SK, Sonker M. Green synthesis of nanoparticles and their biomedical applications: a review. *ACS Appl Nano Mater*. 2021;4(11):11428–11457. doi:10.1021/acsanm.1c02946

69. Halder U, Roy RK, Biswas R, Khan D, Mazumder K, Bandopadhyay R. Synthesis of copper oxide nanoparticles using capsular polymeric substances produced by Bacillus altitudinis and investigation of its efficacy to kill pathogenic Pseudomonas aeruginosa. *Chem Eng J Adv*. 2022;11:100294. doi:10.1016/j.ceja.2022.100294

70. Khandelwal M, Sharma D, Pemawat G, Khangarot RK. Mechanistic insights into photodegradation of organic dyes using copper oxide nanocatalyst. In: *Current and Future Perspectives of Environmental Pollution and Its Remediation*. Vol. 1. Tamil Nadu: Thanuj International Publishers; 2022:36–49.

71. Wilson CM. Studies and critique of amido black 10B, Coomassie blue R, and fast green FCF as stains for proteins after polyacrylamide gel electrophoresis. *Anal Biochem*. 1979;96(2):263–278. doi:10.1016/0003-2697(79)90581-5

72. Wilson CM. Staining of proteins on gels: comparisons of dyes and procedures. In: *Methods in Enzymology*. Vol. 91. Academic Press; 1983:236–247.

73. Pagga U, Brown D. The degradation of dyestuffs: part II Behaviour of dyestuffs in aerobic biodegradation tests. *Chemosphere*. 1986;15(4):479–491. doi:10.1016/0045-6535(86)90542-4

74. Mittal A, Thakur V, Gajbe V. Adsorptive removal of toxic azo dye Amido Black 10B by hen feather. *Environ Sci Pollut Res*. 2013;20(1):260–269. doi:10.1007/s11356-012-0843-y

75. Kashyap J, Gautam S, Ashraf S, Riaz U. Synergistic performance of sonolytically synthesized Poly (1-naphthylamine)/TiO2 nanohybrids: degradation studies of amido black-10B dye. *ChemistrySelect*. 2018;3(42):11926–11934. doi:10.1002/slct.201802688

76. Borker P, Gaokar RD. Enhanced photocatalytic activity of ZnO supported on Alumina and Antibacterial study. *Surf Interfaces*. 2020;19:100477. doi:10.1016/j.surfin.2020.100477

77. Iqbal A, Ahmed AS, Ahmad N, et al. Biogenic synthesis of CeO2 nanoparticles and its potential application as an efficient photocatalyst for the degradation of toxic amido black dye. *Environ Nanotechnol*. 2021;16:100505.

78. Muninathan S, Arumugam S. Enhanced photocatalytic activities of NiS decorated reduced graphene oxide for hydrogen production and toxic dye degradation under visible light irradiation. *Int J Hydrogen Energy*. 2021;46(9):6532–6546. doi:10.1016/j.ijhydene.2020.11.178

79. Jaishree G, Divya G, Rao TS, Chippada M, Raju IM. Biogenic surfactant mediated facile synthesis of visible light sensitized Zn/Mg co-doped TiO2 nanomaterials–a green approach: evaluation of photocatalytic activity by degradation of Amido Black 10B. *Sustainable Environ Res*. 2022;32(1):1–20. doi:10.1186/s42834-022-00149-4

80. Nandiyanto ABD, Zaen R, Oktiani R. Correlation between crystallite size and photocatalytic performance of micrometer-sized monoclinic WO3 particles. *Arabian J Chem*. 2020;13(1):1283–1296. doi:10.1016/j.arabjc.2017.10.010

81. Sharma A, Dutta RK. Studies on the drastic improvement of photocatalytic degradation of acid Orange-74 dye by TPPO capped CuO nanoparticles in tandem with suitable electron capturing agents. *RSC Adv*. 2015;5(54):43815–43823. doi:10.1039/C5RA04179A

82. Vyas Y, Chundawat P, Punjabi PB, Ameta C, Ameta C. Green and facile synthesis of luminescent CQDs from pomegranate peels and its utilization in the degradation of azure B and amido black 10B by decorating it on CuO nanorods. *ChemistrySelect*. 2021;6(33):8566–8580. doi:10.1002/slct.202102156

83. Mousavi M, Habibi-Yangjeh A, Abitorabi M. Fabrication of novel magnetically separable nanocomposites using graphitic carbon nitride, silver phosphate and silver chloride and their applications in photocatalytic removal of different pollutants using visible-light irradiation. *J Colloid Interface Sci*. 2016;480:218–231. doi:10.1016/j.jcis.2016.07.021

84. Pearson RG. Absolute electronegativity and hardness: application to inorganic chemistry. *Inorganic Chemistry*. 1988;27(4):734–740. doi:10.1021/ic00277a030

85. Fouda A, Hassan SED, Saied E, Hamza MF. Photocatalytic degradation of real textile and tannery effluent using biosynthesized magnesium oxide nanoparticles (MgO-NPs), heavy metal adsorption, phytotoxicity, and antimicrobial activity. *J Environ Chem Eng*. 2021;9(4):105346. doi:10.1016/j.jece.2021.105346

86. Kansal S, Singh M, Sud D. Studies on photodegradation of two commercial dyes in aqueous phase using different photocatalysts. *J Hazard Mater*. 2007;141(3):581–590. doi:10.1016/j.jhazmat.2006.07.035

87. Vyas Y, Chundawat P, Dharmendra D, Jain A, Punjabi PB, Ameta C. Biosynthesis and characterization of carbon quantum Dots@ CuS composite using water hyacinth leaves and its usage in photocatalytic dilapidation of Brilliant Green dye. *Mater Chem Phys*. 2022;281:125921. doi:10.1016/j.matchemphys.2022.125921

88. Sravanthi M, Muni Kumar D, Usha B, et al. Biological synthesis and characterization of copper oxide nanoparticles using Antigonon leptopus leaf extract and their antibacterial activity. *Int J Adv Res*. 2016;4(8):589–602. doi:10.21474/IJAR01/1251

89. Kouhkan M, Ahangar P, Babaganjeh LA, Allahyari-Devin M. Biosynthesis of copper oxide nanoparticles using Lactobacillus casei subsp. casei and its anticancer and antibacterial activities. *Curr Nanosci*. 2020;16(1):101–111. doi:10.2174/1573413715666190318155801

90. Azam A, Ahmed AS, Oves M, Khan MS, Habib SS, Memic A. Antimicrobial activity of metal oxide nanoparticles against Gram-positive and Gram-negative bacteria: a comparative study. *Int j Nanomed*. 2012;7:6003. doi:10.2147/IJN.S35347

91. Kalaiyan G, Suresh S, Thambidurai S, et al. Green synthesis of hierarchical copper oxide microleaf bundles using Hibiscus cannabinus leaf extract for antibacterial application. *J Mol Struct*. 2020;1217:128379. doi:10.1016/j.molstruc.2020.128379

92. Mohan P, Mala R. Comparative antibacterial activity of magnetic iron oxide nanoparticles synthesized by biological and chemical methods against poultry feed pathogens. *Mater Res Express*. 2019;6(11):115077. doi:10.1088/2053-1591/ab4964

93. Wang L, Hu C, Shao L. The antimicrobial activity of nanoparticles: present situation and prospects for the future. *Int J Nanomed*. 2017;12:1227–1249. doi:10.2147/IJN.S121956

94. Applerot G, Lellouche J, Lipovsky A, et al. Understanding the antibacterial mechanism of CuO nanoparticles: revealing the route of induced oxidative stress. *Small*. 2012;8(21):3326–3337. doi:10.1002/smll.201200772

95. Ma X, Zhou S, Xu X, Du Q. Copper-containing nanoparticles: mechanism of antimicrobial effect and application in dentistry-a narrative review. *Front Surg*. 2022;9:905892. doi:10.3389/fsurg.2022.905892